The Broad Role of Nkx3.2 in the Development of the Zebrafish Axial Skeleton

Laura Waldmann[1,a], Jake Leyhr[1,a], Hanqing Zhang[2,3], Caroline Öhman-Mägi[4], Amin Allalou[2,3], Tatjana Haitina[1*]

Affiliations

[1] Subdepartment of Evolution and Development, Department of Organismal Biology, Uppsala University, 75236 Uppsala, Sweden.

[2] Division of Visual Information and Interaction, Department of Information Technology, Uppsala University, 75105 Uppsala, Sweden

[3] Science for Life Laboratory BioImage Informatics Facility, Uppsala, Sweden

[4] Division of Applied Materials Science, Department of Engineering Sciences, Uppsala University, 751 21 Uppsala, Sweden.

* corresponding author: Tatjana Haitina, e-mail: tatjana.haitina@ebc.uu.se

[a] These authors contributed equally

Keywords: nkx3.2, bapx1, zebrafish, jaw joint, axial skeleton, occipital, basiventral cartilage, fin radials, CRISPR/Cas9 mutant

Abstract

The transcription factor Nkx3.2 (Bapx1) is an important chondrocyte maturation inhibitor. Previous *Nkx3.2* knock-down and overexpression studies in non-mammalian gnathostomes have focused on its role in primary jaw joint development, while little is known about the function of this gene in broader skeletal development. We generated CRISPR/Cas9 knockout of *nkx3.2* in zebrafish and applied a range of techniques to characterize skeletal phenotypes at developmental stages from larva to adult, revealing fusions in bones of the occiput, the loss or deformation of bony elements derived from basiventral cartilages of the vertebrae, and an increased length of the proximal radials of the dorsal and anal fins. These phenotypes are reminiscent of *Nkx3.2* knockout phenotypes in mammals, suggesting that the function of this gene in axial skeletal development is ancestral to osteichthyans. Our results highlight the broad role of *nkx3.2* in zebrafish skeletal development and its context-specific functions in different skeletal elements.

Introduction

NK3 homeobox 2 (Nkx3.2, Bapx1) is an evolutionarily conserved gene encoding a homeodomain-containing transcription factor that is involved in cartilage growth and differentiation in gnathostomes. It was first described in Drosophila (*bagpipe, bap*), where it plays a major role in the visceral mesoderm during the formation of the midgut musculature (Azpiazu and Frasch, 1993). During vertebrate evolution *Nkx3.2* expression was incorporated into the intermediate domain of the first pharyngeal arch. This event has been proposed to be crucial for jaw joint formation during the transition from jawless to jawed vertebrates (Cerny et al., 2010). Jawed vertebrates like the zebrafish, frog, and chicken display a focal expression of *Nkx3.2* between Meckel's and palatoquadrate cartilages of the first pharyngeal arch skeleton in contrast to the jawless lamprey, which shows more diffuse expression (Kuraku et al., 2010; Miller et al., 2003; Square et al., 2015; Wilson and Tucker, 2004). During development, ventrally migrating cranial neural crest cells form the first pharyngeal arch skeleton. This process is controlled by signalling molecules like endothelin-1 (Edn1), which positively regulates Nkx3.2 (Miller et al., 2003; Nair et al., 2007). Previous studies showed that Nkx3.2 is an essential factor for primary jaw joint development, as the loss of expression in zebrafish, frog, and chick leads to a failure in jaw joint formation accompanied by the fusion of the joint articulating cartilage elements: Meckel´s cartilage and the palatoquadrate (Lukas and Olsson, 2018a; Miller et al., 2003; Wilson and Tucker, 2004). Overexpression of *nkx3.2* (*bapx1*) in amphibians induces the formation of ectopic cartilage elements by introducing additional subdivisions into existing cartilage, clearly showing the joint-promoting effect of this transcription factor (Lukas and Olsson, 2018b).

As a consequence of the primary jaw joint to middle ear transition during the course of mammalian evolution (Luo, 2011; Anthwal *et al*., 2013), *Nkx3.2* is expressed within the middle ear-associated bones of the tympanic ring and gonium as well as in the incudomalleolar joint in mammals (Tucker et al., 2004). Further expression analysis in mouse embryos showed *Nkx3.2* expression in the developing vertebrae and the cartilaginous condensations of the developing limbs (Tribioli et al., 1997). Mouse embryos deficient in *Nkx3.2* display hypoplasia in the tympanic ring, the absence of the gonium, a size reduction of cranial occipital bones such as the basioccipital and basisphenoid, and finally the loss of the supraoccipital bone and vertebral ossification centres (Lettice et al., 1999; Tribioli and Lufkin, 1999; Tucker et al., 2004). Various studies describe Nkx3.2 as a chondrocyte maturation inhibitor during chondrogenesis (Caron et al., 2013; Lengner et al., 2005; Provot et al., 2006; Yamashita et al., 2009). In chicken and mouse long bone development, Nkx3.2 can repress the chondrocyte maturation factor Runx2 during endochondral ossification and thus maintaining the chondrocytes in an immature state (Provot et al., 2006). In humans the homozygote mutation in NKX3.2 gene leads to a spondylo-megaepiphyseal-metaphyseal dysplasia (SMMD), a rare skeletal disease (Hellemans et al., 2009; Simsek-Kiper et al., 2019). The patients suffer from, among other symptoms, a short stature, stiff neck and trunk, and defects in vertebral ossification (Agarwal et al., 2003; Hellemans et al., 2009; Silverman and Reiley, 1985; Simon et al., 2012; Simsek-Kiper et al., 2019), similar to what was observed in mouse knockout mutants. These data clearly indicate a role of Nkx3.2 in the mammalian axial skeleton beyond just the middle ear that is homologous to the non-mammalian primary jaw joint, and yet the function of this gene in the axial skeleton of non-mammals has not been investigated in detail. In zebrafish embryos and juveniles *nkx3.2* expression can be

84 detected in the anterior notochord, vertebrae, and median proximal radials (Arnold et al.,
85 2015; Crotwell and Mabee, 2007).
86
87 In this study, we present a comprehensive investigation of the function of *nkx3.2* in zebrafish
88 skeletal development by generating a CRISPR/Cas9 induced mutant line and characterizing
89 larval, juvenile, and adult phenotypes. Our results confirm and elaborate on the primary jaw
90 joint loss previously reported in knockdown studies and we describe novel axial phenotypes
91 in the occiput, Weberian apparatus, rib-bearing vertebrae, and median fins, pushing back
92 the likely origin of axial functions of Nkx3.2 to the osteichthyan stem group.
93
94
95 **Results**
96 *Zebrafish nkx3.2$^{uu2803/uu2803}$ line generated with CRISPR/Cas9 survives to adulthood and has*
97 *open mouth phenotype*
98 Clustered Regulatory Interspaced Short Palindromic (CRISPR)/CRISPR-associated protein 9
99 (Cas9) was used to generate *nkx3.2* mutant line to analyse both embryonic and adult mutant
100 phenotypes. We generated a mutant line with a 7 bp deletion in *nkx3.2* exon 1 (c.286_292
101 del, p.Lys95*), causing a frameshift, which resulted in a premature stop codon that shortens
102 the peptide sequence to 95 amino acids, compared to 245 amino acids in the wild-type
103 (Figure 1A-B). The DNA-binding homeodomain of Nkx3.2 is absent in this shortened protein.
104
105 Heterozygous embryos (*nkx3.2*$^{uu2803/+}$) displayed no morphological differences compared to
106 wild-type (*nkx3.2*$^{+/+}$) embryos as long as observed (data not shown). Homozygous mutant
107 embryos displaying morphological differences were generated by crossing two heterozygous

nkx3.2$^{uu2803/+}$ adult zebrafish. Homozygous mutants (*nkx3.2*$^{uu2803/uu2803}$) were able to survive to adulthood and displayed a prominent fixed open mouth phenotype (Figure 1C). Adult homozygous mutants displayed differences in size relative to adult wild-type, although it was difficult to determine whether this was due to the mutation or a consequence of the fixed open mouth phenotype effect on feeding (Figure S1).

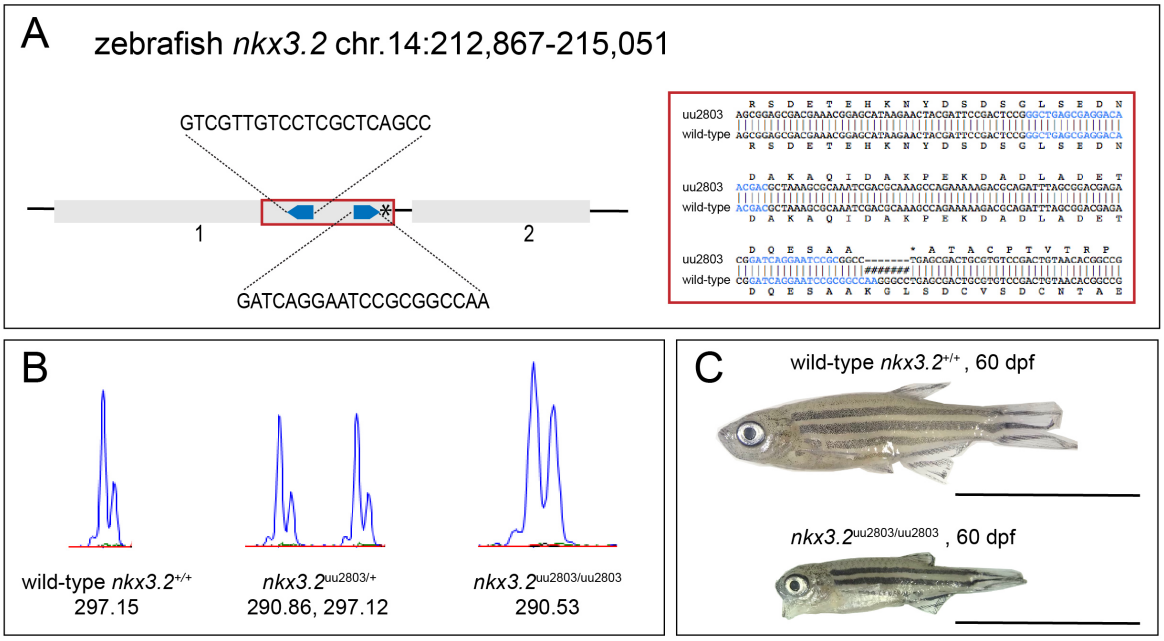

Figure 1 – Zebrafish *nkx3.2* knockout generated with CRISPR/Cas9. (**A**) Schematic diagram of zebrafish *nkx3.2* exons one and two marked by grey rectangles with two CRISPR target sides marked by blue arrowheads. The 7 bp deletion in the first exon is marked by the asterisk in exon 1. The deletion causes an early a stop codon after 95 amino acids (confirmed by sequencing) (**B**) Wild-type, heterozygous *nkx3.2*$^{uu2803/+}$ and homozygous *nkx3.2*$^{uu2803/uu2803}$ fish were analysed by fragment length analysis. The wild-type displayed one peak (297,15), *nkx3.2*$^{uu2803/+}$ fish one wild-type (297,12) and one mutant peak (290,86) and *nkx3.2*$^{uu2803/uu2803}$ fish one mutant peak (290,53). (**C**) At 60 dpf *nkx3.2*$^{uu2803/uu2803}$ fish display a prominent fixed open mouth phenotype. Scale bars: 1 cm.

Confocal live imaging displays fusion of Meckel's cartilage with palatoquadrate in nkx3.2$^{uu2803/uu2803}$ *zebrafish embryo and larvae*

In order to follow the effects of *nkx3.2* CRISPR/Cas9 induced knockout within the first mandibular arch during development, confocal live imaging was performed. To visualise the pharyngeal arches, Tg(*sox10:egfp*) line labelling neural crest-derived cells was used. Clear

129 phenotypic differences in the jaw joint-forming region were detectable from 3 dpf onwards
130 (Figure 2). The jaw joint was lost in *nkx3.2*$^{uu2803/uu2803}$ fish as Meckel's cartilage and the
131 palatoquadrate were fused (Figure 2 E-H´) and the retroarticular process (RAP) was missing
132 at the posteroventral tip of Meckel's cartilage (Figure 2). Knockout of *nkx3.2* furthermore
133 resulted in an unorganised cell-mass of small rounded chondrocytes in the area where the
134 jaw joint is normally formed at 3 and 5 dpf, whereas chondrocytes of Meckel's cartilage and
135 the palatoquadrate more distal to the jaw joint-forming region were elongated and
136 displayed typical stacking (Figure 2 E, E´, F, F´). By 7 dpf, chondrocytes at the fusion site
137 acquired a more elongated shape and began to align with the stacked chondrocytes of
138 Meckel´s cartilage and the palatoquadrate (Figure 2 G, G´). At 14 dpf, all chondrocytes at the
139 fusion site were elongated and aligned completely with the adjacent chondrocytes (Figure 2
140 H, H´).

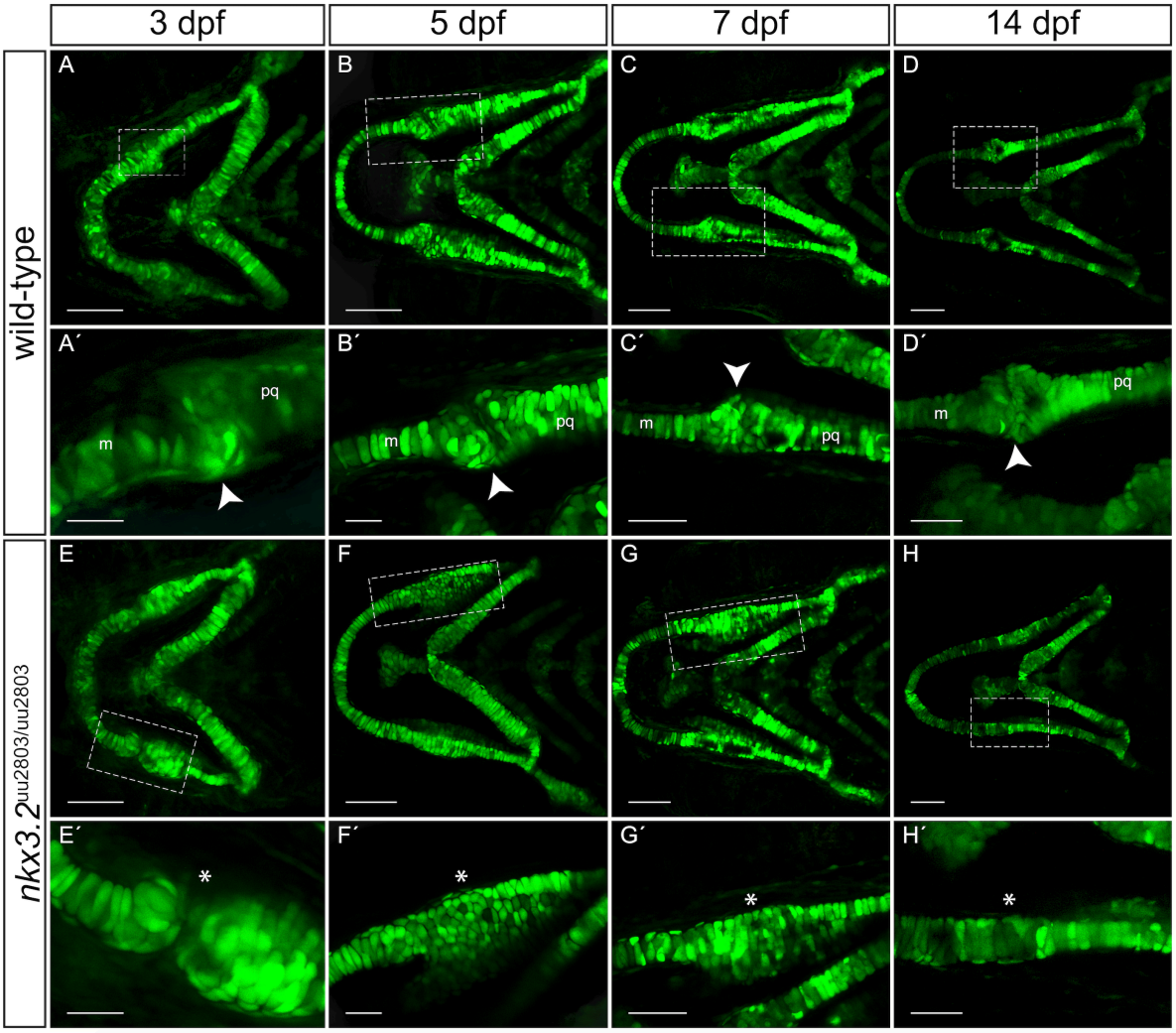

Figure 2 – Larval development of wild-type and *nkx3.2*$^{uu2803/uu2803}$ jaw joints. (**A-H'**) Maximum projections of confocal live imaging Z stacks acquired from ventral side of wild-type zebrafish head at 3 dpf (**A, A'**), 5 dpf (**B, B'**), 7dpf (**C, C'**), 14 dpf (**D, D'**) and *nkx3.2*$^{uu2803/uu2803}$ zebrafish head at 3 dpf (**E, E'**), 5 dpf (**F, F'**), 7 dpf (**G, G'**), 14 dpf (**H, H'**) in Tg(*sox10:egfp*) background. (**A-D**) The jaw joint in wild type zebrafish (dashed box) is magnified in **A'-D'**. The retroarticular process is visible from 3 dpf onwards, marked by white arrowhead. Chondrocytes of Meckel's cartilage and palatoquadrate align in stacks. Posterior Meckel's cartilage and anterior palatoquadrate articulate the jaw joint. (**E-H**) Fusion of jaw joint articulating elements in *nkx3.2* mutant fish. The fusion is magnified in (**E'-H'**) and indicated by asterisks. (**E'-F'**) 3 dpf and 5 dpf *nkx3.2* mutant embryos display unorganised and rounded cells in the area where the joint would normally form. (**G'**) 7 dpf *nkx3.2* mutant larvae display elongated cells in the fused area, which starts to align in stacks. (**H'**) 14 dpf *nkx3.2* mutant zebrafish display elongated cells that align with adjacent Meckel's cartilage and palatoquadrate. m - Meckel's cartilage, pq - palatoquadrate. Scale bars: 100 μm (**A-H**), 25 μm in (**A'-H'**).

Histological analysis of nkx3.2$^{uu2803/uu2803}$ *zebrafish shows chondrocyte alignment and hypertrophy at the jaw joint fusion site*

160 Histological sections were prepared to further analyse the chondrocyte arrangement within
161 the first mandibular arch in *nkx3.2* mutant larval, juvenile, and adult zebrafish. A joint gap
162 between Meckel´s cartilage and the palatoquadrate is visible in wild-type zebrafish at 14 dpf.

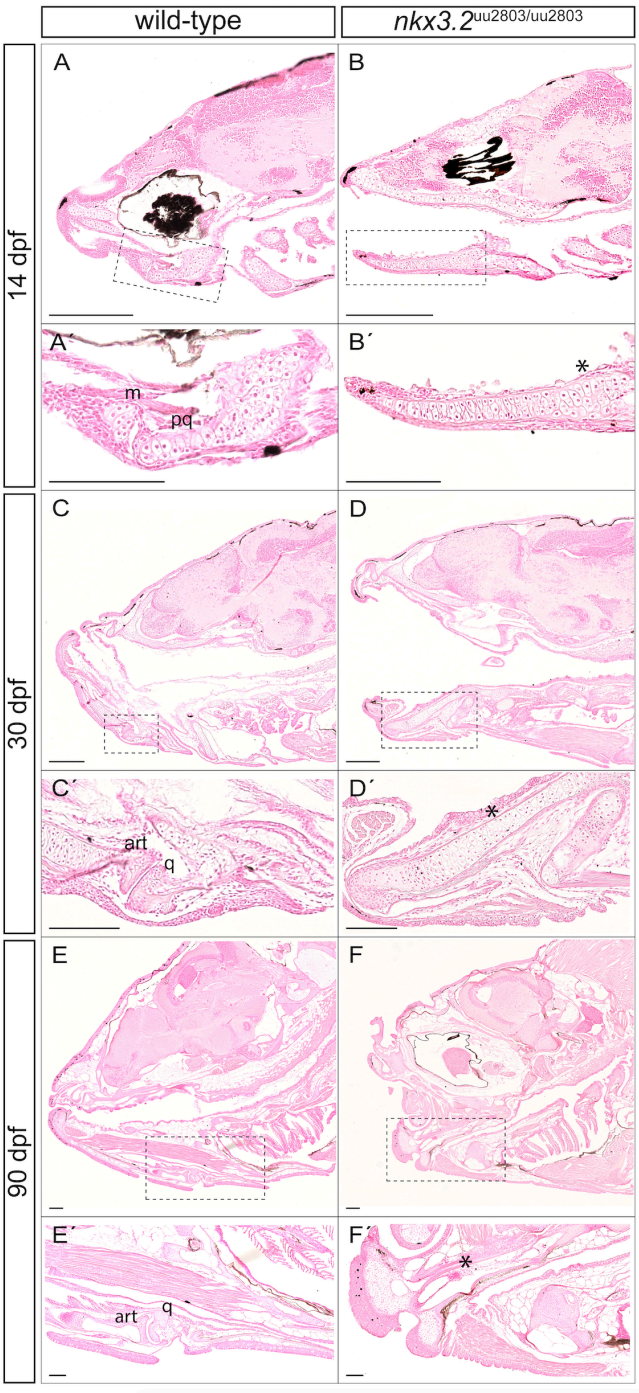

163

164 **Figure 3 – Histological analysis reveals loss of jaw joint without affected chondrocyte**
165 **hypertrophy in the first pharyngeal arch of *nkx3.2*$^{uu2803/uu2803}$ zebrafish.** Sagittal sections of
166 wild-type 14 dpf (**A, A'**), 30 dpf (**C, C'**) and 90 dpf (**E, E'**) and *nkx3.2* mutant 14 dpf (**B, B'**) 30
167 dpf (**D, D'**) and 90 dpf (**F, F'**) zebrafish stained with Nuclear Red Stain. (**A, A', C, C', E, E'**)
168 Stained histology sections displaying a normal jaw joint development between Meckel's

cartilage (m) and palatoquadrate (pq), respectively articular (art) and quadrate (q) in wild-type fish. (**B, B', D, D', F, F'**) *nkx3.2* mutant fish do not display a jaw joint. Chondrocyte maturation and ossification seem not to be affected in *nkx3.2*$^{uu2803/uu2803}$ besides the absence of joint-typical cells lining the articulating elements. Dashed box in (**A-F)** marks the magnified region in (**A'-F')**. Asterisk mark the jaw joint fusion. m – Meckel's cartilage, pq – palatoquadrate, art – articular, q – quadrate. Scale bars: 200μm (**A-F**), 100μm (**A'-F'**).

Articular chondrocytes lining the joint cavity and hypertrophic chondrocytes forming the articulating elements were present (Fig. 3 A and A´). In *nkx3.2* mutant larvae at 14 dpf, Meckel´s cartilage and the palatoquadrate were not separated but fused – the jaw joint was absent. Chondrocytes within the fused element were hypertrophic and aligned. At the presumptive fusion site, the element appeared to be increased in width caused by piled-up rows of aligned chondrocytes (Fig.3 B and B´). The exact fusion point was difficult to determine in both 30 dpf and 90 dpf mutant fish but apart from the fusion and its phenotypic consequences, ossification seemed not to be affected. Articular chondrocytes lining the articulating tips of the articular and quadrate were consequently absent in *nkx3.2* mutant juvenile fish at 30 dpf. Chondrocytes within the fused element underwent hypertrophy as in wild-type fish (Fig. 3 C-D´). By 90 dpf, ossification of the fused articular and quadrate was completed, visible by the presence of adipose tissue inside the bones in both wild-type and mutant adult fish (Fig. 3 E-F´).

Optical projection tomography reveals morphological changes in the head of *nkx3.2*$^{uu2803/uu2803}$ *larvae*

In order to characterise the larval *nkx3.2* mutant phenotype in greater detail, we used optical projection tomography (OPT) on 5 dpf cartilage-stained larvae to reconstruct 3D models of wild-type and mutant cartilage morphology. Multiple wild-type (n=10) and mutant (n=11) 3D models were overlaid and combined to produce an average wild-type morphology

(Figure 4A, D, G) and an average *nkx3.2* mutant morphology (Figure 4B, E, H). Overlaying these grouped 3D reconstructions allowed the calculation of voxels that were statistically more or less intense in the mutant group, corresponding to locations with more or less cartilage present, respectively. This analysis was robust to false positives (Figure S2).

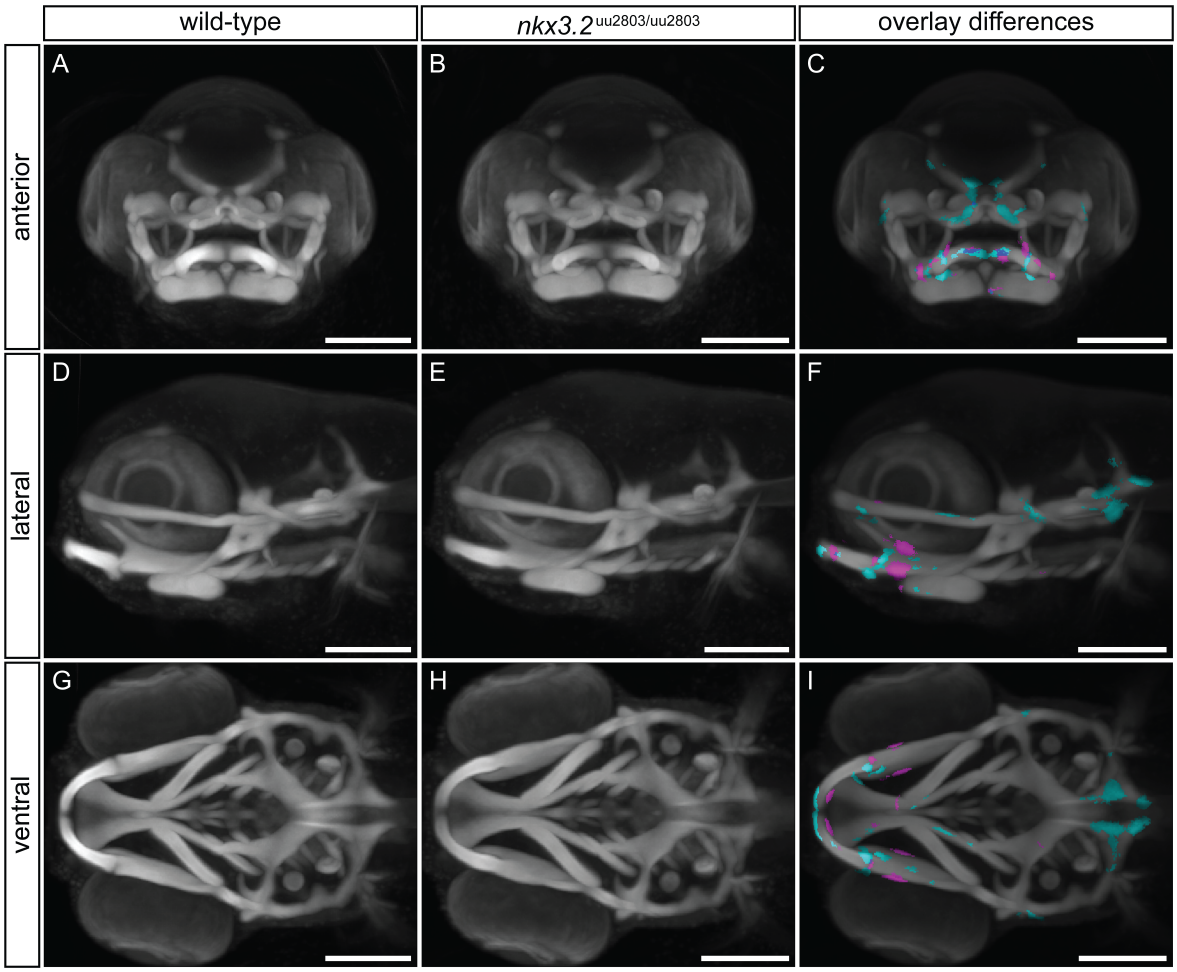

Figure 4 – Optical projection tomography of cartilage-stained wild-type and *nkx3.2 uu2803/uu2803* larvae reveals subtle phenotypic changes. (**A, D, G**) Maximum projection of 5 dpf wild-type group (n=10). (**B, E, H**) Maximum projection of 5 dpf *nkx3.2* mutant (n=11) group. (**C, F, I**) Maximum projection of both groups with coloured voxels representing voxels with statistically significant ($p<2.5x10^{-4}$) differences in intensity. Cyan shows voxels with lower intensity and magenta shows voxels with higher intensity in *nkx3.2* mutant group. Scale bars: 300µm.

The *nkx3.2* mutant group showed significantly higher intensity of the cartilage labelling at the jaw joint region (magenta in Figure 4F, I) consistent with the presence of fused cartilage

in mutants compared to the jaw joint gap in wild-type larvae. Cyan voxels ventral to the jaw joint in Figure 4F indicate the absence of the RAP. The palatoquadrate displayed significantly higher intensity in *nkx3.2* mutant group consistent with the increased thickness of this element (magenta in Figure 4C, F, I). The anterior part of Meckel's cartilage displayed an increased posterior intensity and decreased anterior intensity in the *nkx3.2* mutant group indicating a subtle change in the shape of Meckel's cartilage (Figure 4I). Interestingly, this analysis also revealed significantly reduced cartilage staining signal in the posterior part of the head, around the otic capsule (Figure 4 F, I). The mutant group clearly showed the shorter parts of the auditory capsule and thinner parachordal changing the shape of the notochord insertion, compared to the wild-type group (Figure 4F, I).

Cartilage and bone staining analysis of wild-type and nkx3.2$^{uu2803/uu2803}$ larval, juvenile and adult zebrafish

Skeletal staining of larval, juvenile and adult *nkx3.2* mutant zebrafish was performed to analyse both cartilage and bone abnormalities in comparison to wild type at a greater range of developmental stages. The loss of the jaw joint caused by the fusion of Meckel´s cartilage and palatoquadrate was clearly visible from 5 dpf onwards and was most recognizable by the absence of the RAP (Figure 5). The resulting open mouth phenotype could be observed from 9 dpf onwards (Figure 5D, F, H). No other cartilage phenotypes within the pharyngeal arches could be detected at any developmental stage, consistent with the OPT results at 5 dpf in Figure 4. Ossification of the dentary, articular, and quadrate appeared to take place normally in *nkx3.2* mutants at 30 dpf (Figure 5H') when compared to wild-type fish (Figure 5G'), although the absence of the cartilaginous jaw joint resulted in an ossified fusion between the articular and quadrate.

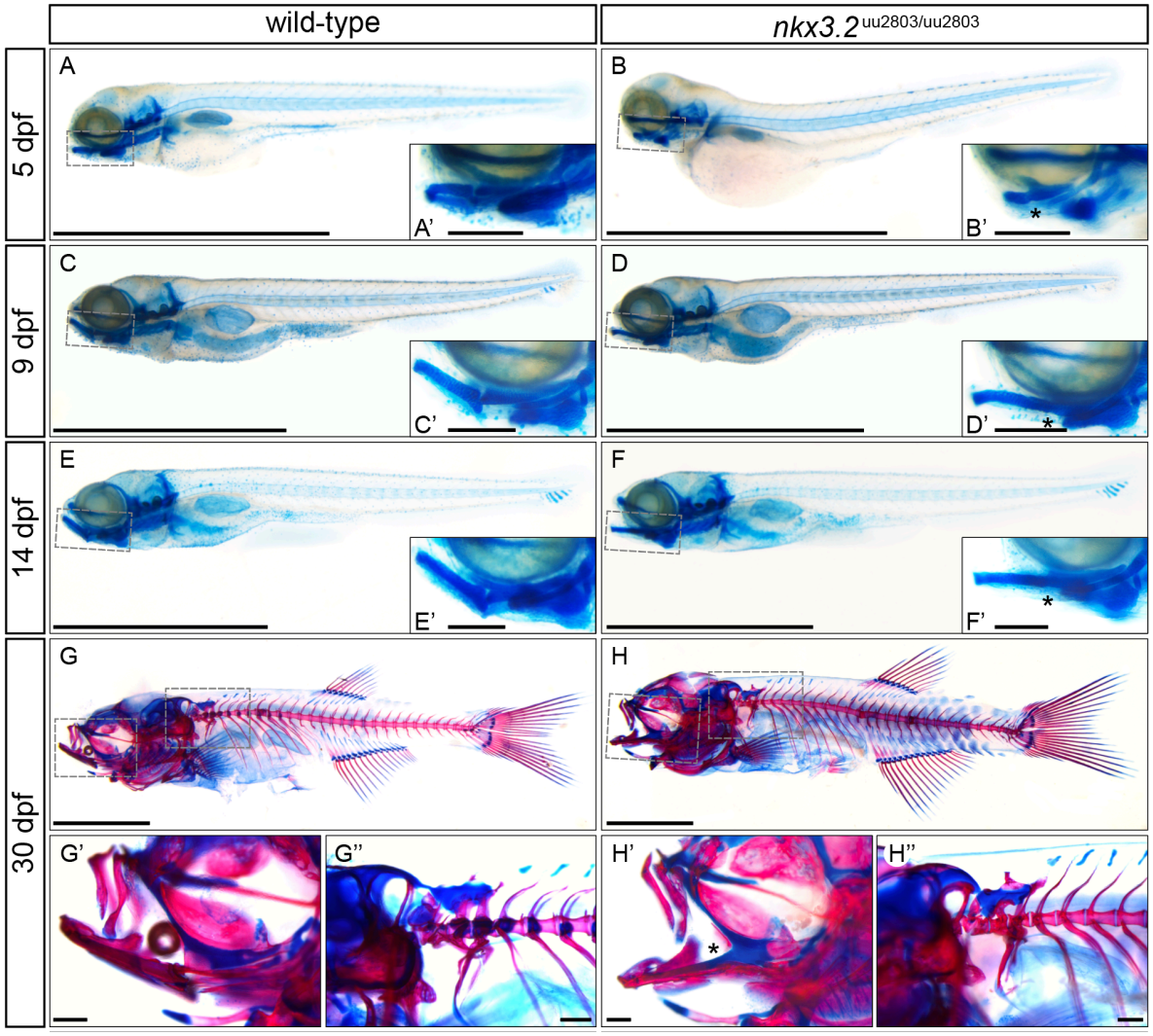

Figure 5 – Skeletal staining of wild-type and *nkx3.2*$^{uu2803/uu2803}$ zebrafish. (**A-F**) lateral views of cartilage-stained wild-type and *nkx3.2* mutants from 5-14 dpf. (**G-H**) lateral views of cartilage- and bone-stained wild-type and *nkx3.2* mutants at 30 dpf. Boxes in (**A-H**) indicate the zoomed-in regions in the insets or zoomed-in panels (**G'**, **G''**, **H'**, **H''**). Asterisks indicate the fusion between Meckel's cartilage and palatoquadrate in the jaw joint. Scale bars: 2mm (**A-H**), 200µm (**A'-H''**).

µCT reveals craniofacial phenotypes in adult nkx3.2$^{uu2803/uu2803}$ *zebrafish*

In order to examine the axial skeleton of adult zebrafish we performed µCT followed by 3D reconstruction of wild-type and *nkx3.2* mutant zebrafish at 90 dpf (Figure 6). The resting position of the mouth is closed (CM) in wild-type individuals, so to be better able to compare

247 the phenotype of the wild-type to the open-mouthed mutant, µCT scans were also
248 performed on 90 dpf zebrafish with their mouths held open (OM) with a pipette tip.
249 The fusion of the Meckel's and palatoquadrate cartilages early in the development of
250 *nkx3.2* mutants effectively resulted in a fusion of the articular and quadrate that ossify from
251 these cartilage precursors. This made it extremely challenging to demarcate the articular and
252 quadrate in the *nkx3.2* mutants at 90dpf, which is why the lower jaw was not segmented in
253 red in Figure 6B, E, H, K. As in younger *nkx3.2* mutants (Figure 5D, F, H), the mouth of 90dpf
254 mutants was fixed in an open position, and this resulted in opposing forces being exerted
255 between the lower jaw, the basihyal, and the second pharyngeal arch, the ceratohyal. The
256 outcome of these forces varied between different individuals. Figure 6E shows an individual
257 where the ventral position of the lower jaw appeared to have pushed the basihyal and
258 ceratohyal posteroventrally, resulting in a sharp angle between the anteroventrally-pointing
259 anterior end of the ceratohyal and the posteroventrally-pointing posterior end of the
260 basihyal. Other individuals (not shown) had a relatively normal position of the basihyal and
261 ceratohyal in the mouth compared to the ventrally-positioned lower jaw, resulting in the
262 basihyal partially obstructing the open mouth, its anterior end positioned dorsally to the
263 entire lower jaw. In some cases, the opposing forces exerted by the lower jaw and
264 ceratohyal on either side of the basihyal caused it to bend and ossify into an L-shape.

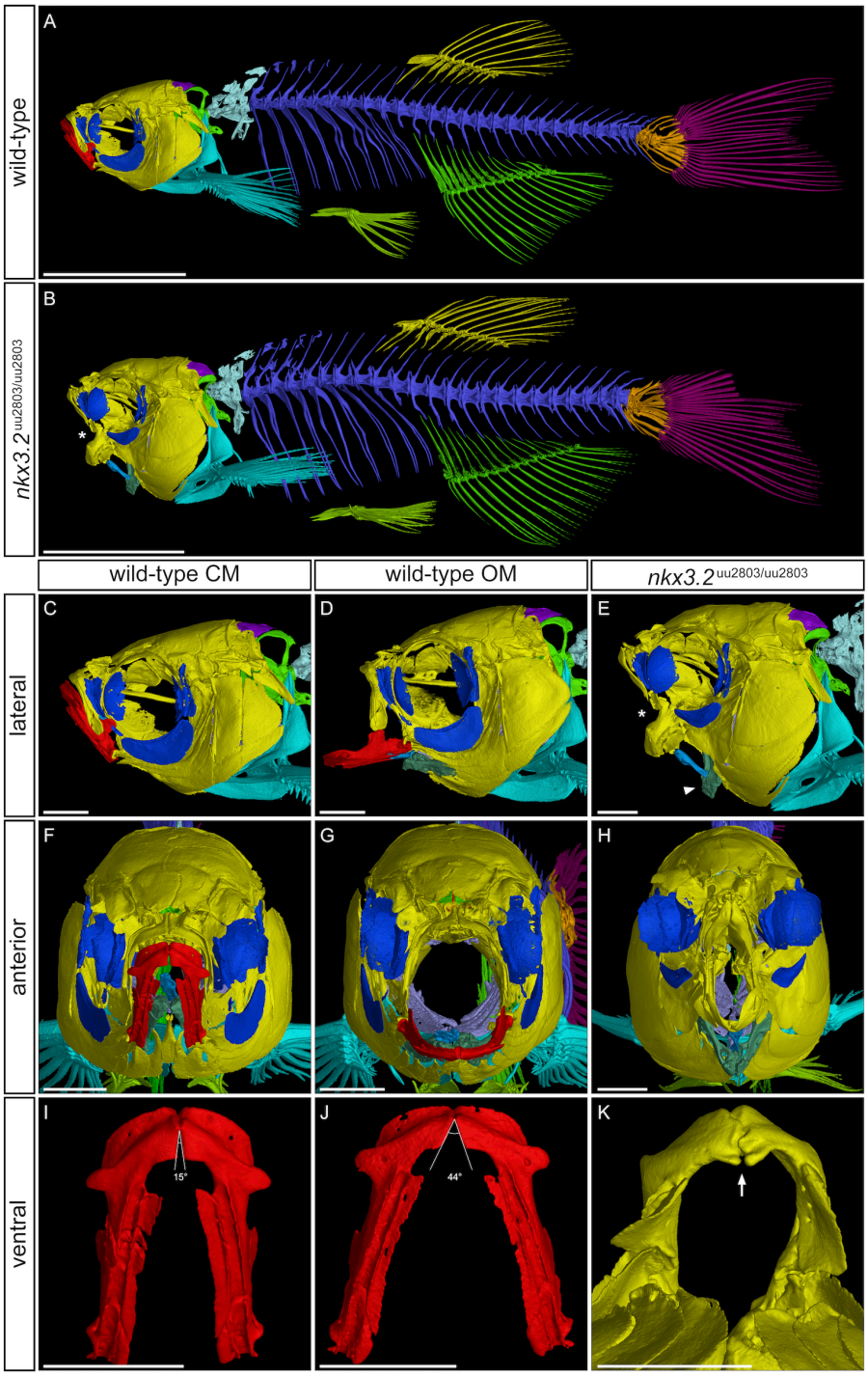

Figure 6 – µCT reveals craniofacial phenotypes in adult wild-type and *nkx3.2*$^{uu2803/uu2803}$ zebrafish. (**A, B**) lateral view of wild-type and *nkx3.2* mutant zebrafish at 90dpf. (**C, D, E**) lateral view of the head of wild-type with closed mouth (CM), wild-type with open mouth (OM), and *nkx3.2* mutant. (**F, G, H**) Anterior view of wild-type with CM, wild-type with OM, and *nkx3.2* mutant. (**I, J, K**) ventral view of isolated wild-type dentary (CM), wild-type dentary (OM), and *nkx3.2* mutant dentary. Asterisks in (**B**, **E**) indicate the fused jaw joint phenotype, the arrowhead in (**E**) indicates the downturned ceratohyal phenotype relative to (**D**). Angles in (**I**, **J**) show the flexibility of the symphysis in wild-type adults, the arrow in (**K**) indicates the deformed symphysis phenotype in *nkx3.2* mutant. Colour scheme: red – lower jaw; dark blue – infraorbitals, lateral ethmoid, and pterosphenoid; dark green – ceratohyal;

blue – basihyal; violet – branchial arches; dark purple – supraoccipital; green – exoccipital and basioccipital; cyan – cleithrum and pectoral fins. Scale bars: 5mm (**A**, **B**), 1mm (**C**-**K**).

Viewed anteriorly (Figure 6F-H), the face of the mutant appeared "pinched" at the position where the jaw joint would have formed, resulting in a reduced area of the mouth opening and an anteromedial rotation of more posterior structures, most notably the pterosphenoid, lateral ethmoid, and infraorbital 3. There were also impacts on the bones of the upper jaw, the premaxilla and maxilla, which also appeared to be posteriorly compressed into the cranium (note the reduced distance between the lateral ethmoid and maxilla in figure 6E relative to 6C, D) and compressed laterally in line with the "pinched" jaw apparatus. Contrary to Miyashita et al. (2020), we found that the kinethmoid was present, not absent, at both 60 and 90 dpf, and relatively morphologically unchanged relative to wild-type fish (Figure S3).

The cartilaginous symphysis joint between the paired bones of the dentary flexes during feeding in wild-type zebrafish as the jaw is opened and the width of the mouth opening is increased by the lateral flaring of the suspensorium (Gidmark et al., 2012; Westneat, 2006), illustrated in Figure 6I, J. In contrast, the symphysis of *nkx3.2* mutants appeared to be fused (Figure 6K) and was likely inflexible.

Juvenile and adult nkx3.2 $^{uu2803/uu2803}$ zebrafish display loss of basiventral cartilage and parapophyses

Next, we assessed the effect of *nkx3.2* knockout on vertebrae-associated bones and cartilages in juveniles and adults. At 30 dpf mutants displayed a loss of basiventral cartilage in the precaudal rib-bearing vertebrae (Figure 7B) compared to wild-type fish (Figure 7A). At 35 dpf wild-type fish also lacked these cartilages (Figure 7C), as they have been entirely

replaced through endochondral ossification by the parapophyses, small articulating bones that connect the ribs to the vertebrae. However, in both 30 dpf and 35 dpf *nkx3.2* mutants, it was clear that this endochondral ossification of basiventral cartilage had not taken place, as the parapophyses were absent (Figure 7B, D). Instead, the ribs were fused directly to the vertebrae without any articulating process, while other ribs were entirely disconnected to the vertebrae. This phenotype persisted in 90 dpf *nkx3.2* mutant adults, as seen in µCT segmented models and virtual histological sections of the vertebrae (Figure 7E-H). In contrast, the neural arches, zygapophyses, and haemal arches appeared to develop normally.

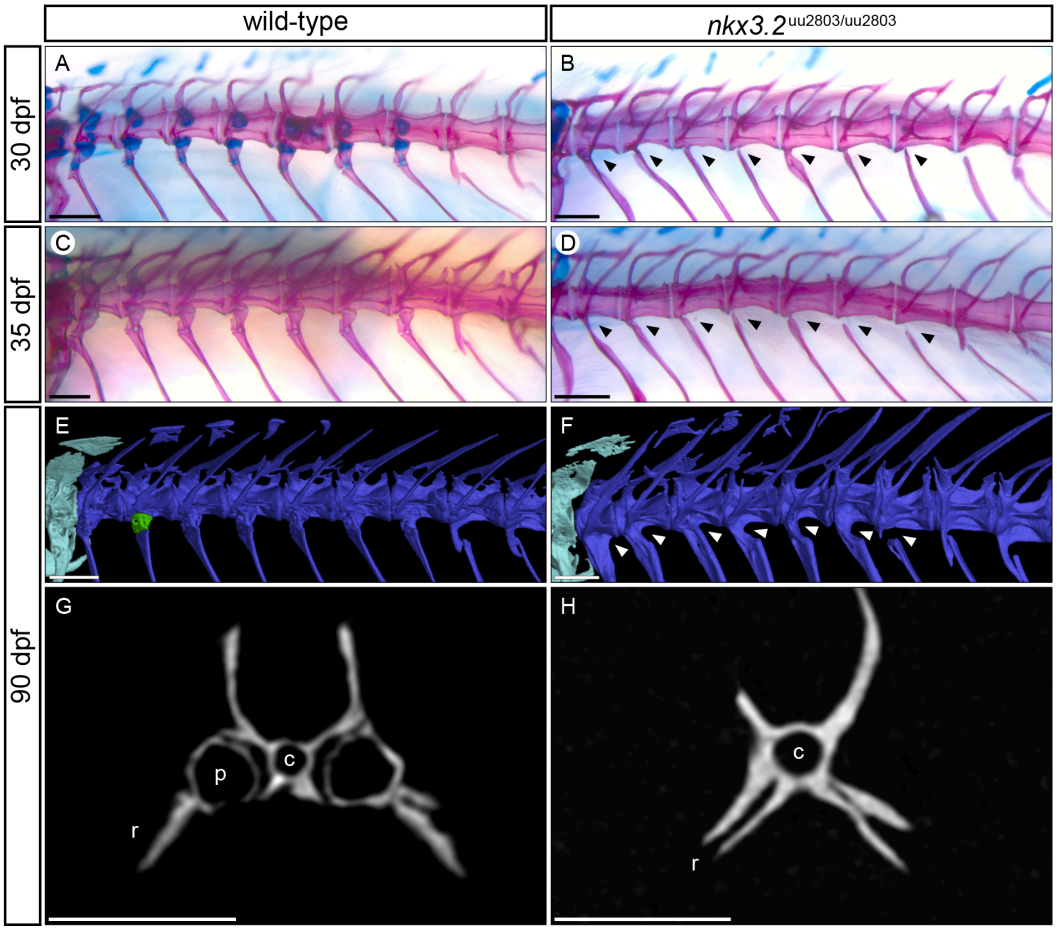

Figure 7 – Parapophyses are absent in the rib-bearing vertebrae of *nkx3.2*$^{uu2803/uu2803}$ zebrafish. (**A-F**) Dorsolateral views of rib-bearing vertebrae in 30, 35, and 90 dpf wild-type and *nkx3.2* mutant zebrafish. (**A-D**) Cartilage- and bone- stained juvenile zebrafish, (**E, F**) µCT models. (**G, H**) µCT virtual transverse cross-sections of wild-type and *nkx3.2* mutant rib-bearing vertebrae at 90 dpf. Arrowheads in (**B, D, F**) indicate the absence of

parapophyses on the rib-bearing vertebrae. A single parapophysis has been highlighted in green in (**E**) as a visual aid. c – centrum, p – parapophysis, r – rib. Scale bars: 200µm(**A-D**), 500µm (**E-H**).

310

311 *OPT, skeletal staining and µCT reveal phenotypes in the occiput and Weberian apparatus of*

312 *nkx3.2*$^{uu2803/uu2803}$ *zebrafish*

313 Comparison of OPT reconstructions of 5 dpf larvae (Figure 4) suggested an effect of *nkx3.2*

314 knockout on some of the cartilage of the otic capsule. At 30 dpf cartilage and bone staining

315 revealed changes in the occipital bones and cervical vertebrae in *nkx3.2* mutant compared to

316 wild-type zebrafish. More specifically, *nkx3.2* mutants displayed smaller lateral occipital

317 fenestrae, due to changes in shapes of exoccipital and supraoccipital as well as reduced

318 cartilages associated with forming Weberian apparatus (Figure 5G'', H'').

319

320 To investigate these phenotypes in greater detail, these bones were segmented from µCT

321 scans of 90 dpf wild-type and *nkx3.2* mutant fish. In the occipital region at the back of the

322 skull, mutants displayed a dramatic fusion between the basioccipital and exoccipital (wild-

323 type is shown in Figure 8A, C, E, G), making it impossible to clearly demarcate these two

324 elements, hence they are the same colour in Figure 8B, D, F, H. A central fissure in the

325 exoccipital (Figure 8E) was also partially or completely fused in mutants (Figure 8F). As a

326 result of the fusion of the central fissure of the exoccipital and between the exoccipital and

327 basioccipital, the posterodorsal opening of the cavum sinus impar (csi) was lost or greatly

328 deformed (Figure 8H). The anteroventral surface of the basioccipital that contacts the

329 parasphenoid and prootic was highly convex in mutants, compared to only slightly convex in

330 wild-types (Figure 8C, D; Figure S4). The posterodorsal exoccipital struts were impacted by

the cervical vertebrae in *nkx3.2* mutants (Figure 8B), causing the lateral occipital fenestrae to be reduced in area and rotated posteromedially.

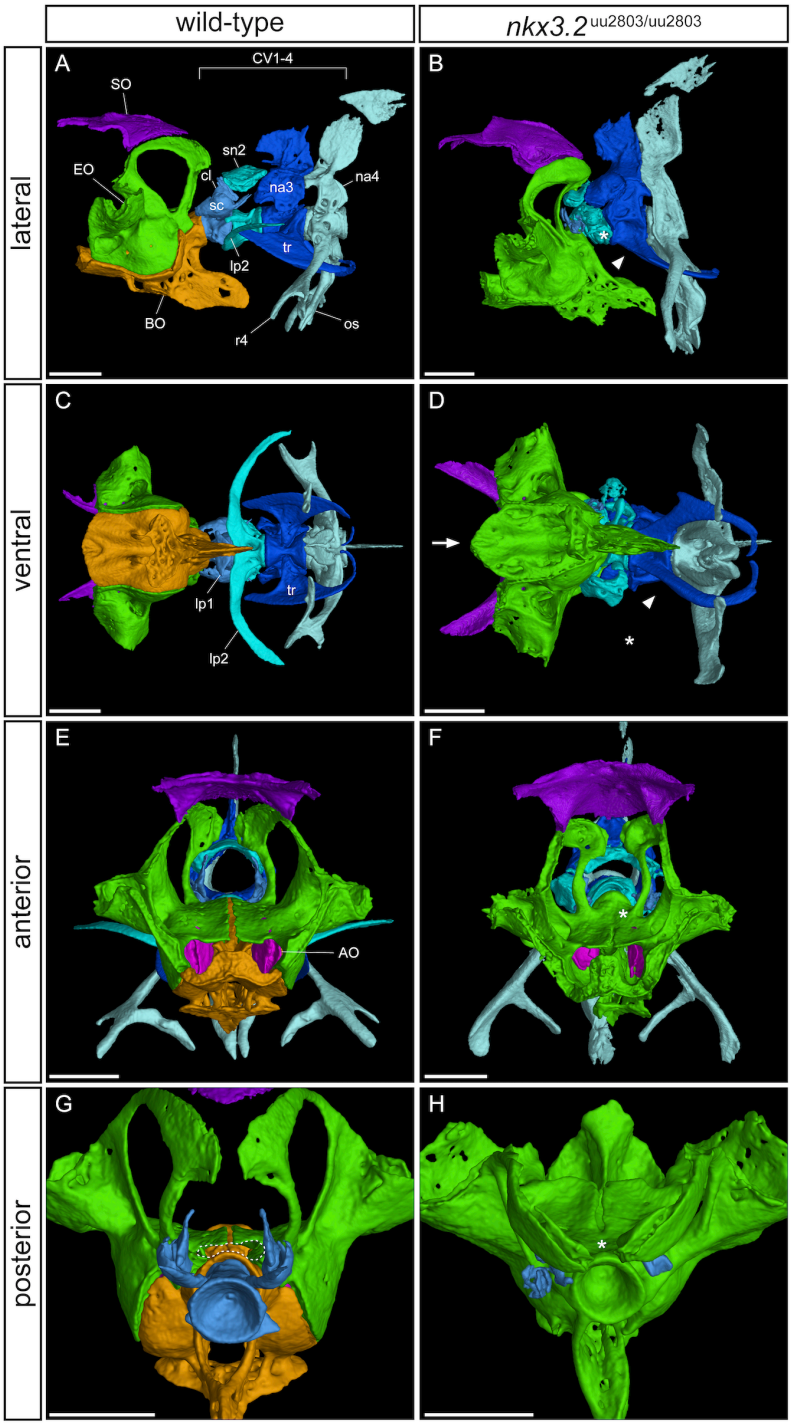

Figure 8 – µCT reveals phenotypes in the occiput and Weberian apparatus of *nkx3.2 uu2803/uu2803* zebrafish. Lateral, ventral, anterior, and posterior views of wild-type (**A, C, E, G**) and homozygous mutant (**B, D, F, H**) occiput and Weberian apparatus. Cervical vertebrae (CV) 2-4 have been removed in (**G, H**) for clarity. Asterisks in (**B**, **D**) indicates the absence or

339 severe reduction of lateral process 2 from CV2, arrowheads indicate absence of anterior
340 ramus of tripus on CV3, arrow indicates the V-shaped anteroventral edge of basipccipital.
341 Asterisk in (**F**) indicates the posterior fusion of the dorsal fissure of the exoccipital. Dotted
342 line in (**G**) highlights the cavum sinus impar (csi), while the asterisk in (**H**) indicates its
343 absence. AO – asteriscus otolith, BO – basioccipital, EO – exoccipital, SO – supraoccipital, cl –
344 claustrum, lp – lateral process, na – neural arch, os – os suspensorium, r4 – rib 4, sc –
345 scaphium, sn2 – supraneural 2, tr – tripus. Scale bars: 500µm.
346

347 Wild-type zebrafish possess four distinct cervical vertebrae (CV), while most mutants lacked
348 the first and most anterior CV (Figure 8A, B), with one mutant also missing CV2. Dorsal to
349 CV1 in wild-type zebrafish lies the scaphium and claustrum, which were entirely lost or
350 highly reduced in all mutants lacking CV1 (Figure 8B, H). The lateral process (lp2) on CV2 was
351 significantly reduced in mutants, varying between individuals from a ~50% reduction in size
352 to almost complete loss (Figure 8D). The tripus of CV3 was deformed in mutants - the
353 anterior ramus and articulating process were absent (Figure 8B, D). The articulation of rib 4
354 and the os suspensorium to CV4 was also altered in mutants, consistent with the absence of
355 parapophyses observed in the rib-bearing vertebrae of vertebrae 5-11 (Figure 7).
356

357 *Proximal radials in the dorsal and anal median fins are longer in nkx3.2$^{uu2803/uu2803}$ compared*
358 *to wild-type adult zebrafish*
359 In order to assess the existence of a mutant phenotype in the dorsal and anal median fins,
360 the lengths of the five anterior-most proximal radials (pr) were measured in µCT images of
361 90 dpf fish, then scaled according to the standard length of each individual to account for
362 body size variation between individuals (Figure 9). These anterior proximal radials were
363 chosen because the radial number is variable even between individuals of the same
364 genotype, so a one-to-one comparison of all radials is not possible. The proximal radials in
365 the anal fin of *nkx3.2* mutants were significantly longer than those in wild-type fish (Figure

9A). Proximal radials of the dorsal fin also tended to be longer, although didn't always reach statistical significance (Figure 9B). These increased radial lengths may partially contribute to the dorsoventrally taller profile of *nkx3.2* mutants. In addition to the increased lengths of these radials, 40% (2/5) of 90 dpf *nkx3.2* mutant fish exhibited a deformity of pr1, such that it appeared to have two shafts (Figure 9D). No such phenotypes were observed in the paired fins or caudal fin, which appeared to develop normally, although these were more challenging to measure.

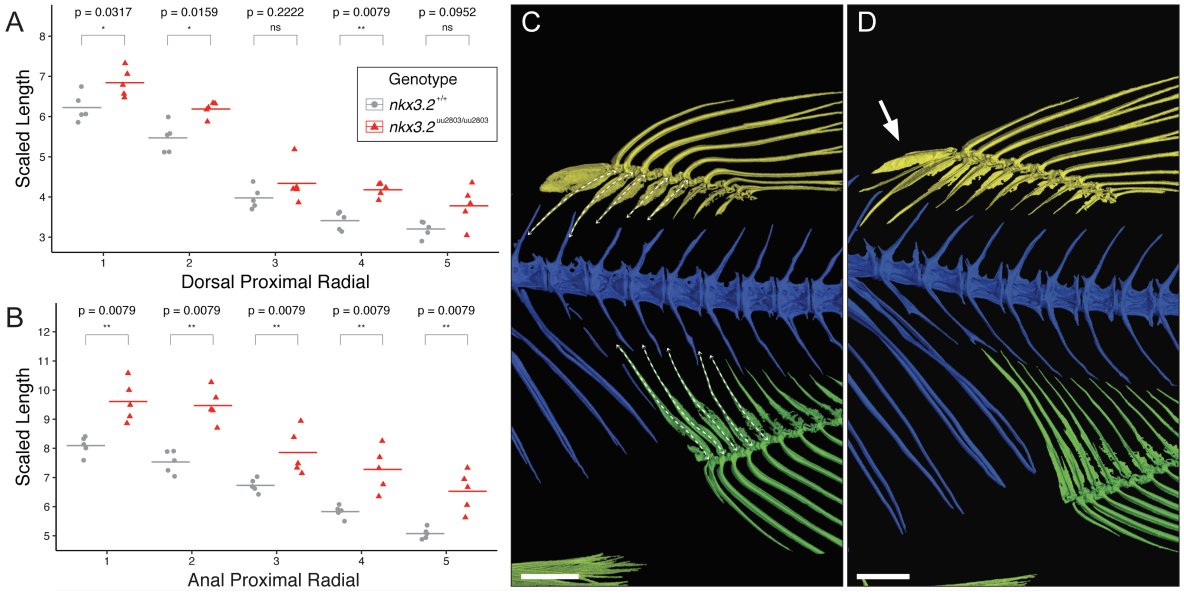

Figure 9 - Proximal radials are longer in adult *nkx3.2* $^{uu2803/uu2803}$ zebrafish. (**A**) Proximal radials 1-5 in the dorsal fin of 90dpf *nkx.3.2* mutants are longer compared to wild-types. (**B**) Proximal radials 1-5 in the anal fin of 90dpf *nkx.3.2* mutants are substantially longer compared to wild-types. Lengths are scaled relative to standard length (SL) of each individual. Horizontal lines represent averages. (**C**) µCT segmented image 90dpf wild-type dorsal (yellow) and anal (green) fins, with white dashed arrows representing the path of the proximal radials measured. (**D**) µCT segmented image 90dpf *nkx3.2* mutant. The arrow indicates a different morphology of proximal radial 1, with the appearance of a duplicated radial shaft. Scale bars: 1mm.

Discussion

In this study, we generated a novel zebrafish knockout mutant of *nkx3.2*. Remarkably, zebrafish homozygous for this mutation survived until adulthood, allowing us to study the mutant phenotype at a range of developmental stages up to and including adults. We employed traditional and novel techniques to characterise the effects on skeletal development this mutation caused. Consistent with previous studies, we identified a key role for nkx3.2 in the development of the jaw joint. However, we also found axial phenotypes that are novel in zebrafish, although they closely mirror phenotypes reported in human and mouse.

Homozygote *nkx3.2* mutant fish displayed a prominent open mouth phenotype from 14 dpf onwards. We did not perform experiments to study the feeding behaviour, but a recent study analysing the open mouth phenotype found that *nkx3.2* mutant fish employ ram feeding (Miyashita et al., 2020). Open mouth in nkx3.2 mutant zebrafish is caused by loss of the jaw joint and as a result, the fusion between Meckel's and palatoquadrate cartilages of the first pharyngeal arch and loss of the retroarticular process (RAP). Our findings are consistent with the previous studies showing expression of *nkx3.2* in the jaw joint of zebrafish (Miller et al., 2003; Schwend and Ahlgren, 2009) and knockdown experiments in both zebrafish and *Xenopus* that result in the fusion of the jaw joint articulating elements Meckel's cartilage and palatoquadrate accompanied by the loss of the retroarticular process (Lukas and Olsson, 2018a; Miller et al., 2003). These results clearly show the importance of Nkx3.2 during primary jaw joint development. Nkx3.2 loss in mouse does not affect the jaw joint but rather the associated bones of the homologous structures present in the middle ear (Tucker et al., 2004).

Our analysis of cellular organization in *nkx3.2* mutant zebrafish larvae showed that, in contrast to wild-type zebrafish, there were no jaw joint progenitor cells that could form the interzone of the jaw joint in *nkx3.2* mutant larvae. It is therefore interesting if nkx3.2 is necessary for interzone formation. Our results are consistent with findings from previous studies describing Nkx3.2 as a chondrocyte maturation inhibiting factor during skeletogenesis, which is able to repress the osteoblast maturation and skeletogenesis factor Runx2 (Lengner et al., 2005; Provot et al., 2006). As Meckel's and palatoquadrate cartilages in *nkx3.2* mutants displayed the alignment of chondrocytes and the ability to become hypertrophic throughout the fused first arch elements. Moreover, in adult mutant zebrafish, fused articular-quadrate displayed typical characteristics of endochondrally ossified spongy bones characterized by adipocytes present in the interspace between the trabeculae (Weigele and Franz-Odendaal, 2016). It is also possible that loss of nkx3.2 could affect another transcription factor barx1. In contrast to nkx3.2, barx1 functions in repressing joint formation and promoting cartilage development. It is expressed in the first pharyngeal arch sub-intermediate domain in wild-type zebrafish, in the cartilage distal to the jaw joint (Nichols et al., 2013). Loss of nkx3.2 may allow the expansion of this expression domain, reinforcing the loss of joint identity in the region. The future examination of altered gene expression patterns of chondrogenic and joint specific factors in *nkx3.2* mutant zebrafish will be beneficial for understanding the jaw joint establishment process during development.

In addition to the primary jaw joint, *nkx3.2* is also expressed in the first arch midline domain – the symphysis joint in zebrafish embryos (Miller et al., 2003; Schwend and Ahlgren, 2009). Optical projection tomography of larvae and skeletal staining of juvenile mutant fish did not

433 detect any abnormalities within this area except a subtle change in the shape of Meckel's
434 cartilage. However, our µCT analysis of the bones of adult mutant fish showed a prominent
435 fusion of the symphysis leading to a distinctive jaw inflexibility. This disruption in symphyseal
436 joint development is reminiscent of altered Hedgehog-signaling pathway in
437 *con/disp1* mutant zebrafish. In these mutants *nkx3.2* expression is absent in the symphysis
438 and reduced in the jaw joint forming region accompanied by the loss of the RAP and fusion
439 of the symphysis (Schwend and Ahlgren, 2009). However, since we could not detect any
440 symphysis defects in larval and juvenile *nkx3.2* mutant fish we suggest that Nkx3.2 is not
441 essential for early symphysis development and the observed adult symphysis fusion could be
442 a consequence of the open mouth phenotype caused by the jaw joint fusion.
443
444 In addition to confirming the essential role of Nkx3.2 in the development of the jaw joint, we
445 describe previously unexplored axial phenotypes associated with *nkx3.2* knockout in
446 juveniles and adults. *nkx3.2* expression in the occiput, vertebrae, and median fins has
447 previously been described (Crotwell and Mabee, 2007), but our analysis of *nkx3.2* knockout
448 phenotypes sheds more light on the specific axial role of this gene.
449
450 The parapophyses that articulate ribs 5-11 with the vertebral centra were absent in juvenile
451 and adult mutants, with many ribs instead ossifying directly onto the centra, and some
452 remaining entirely disconnected from the centra, separated by a gap where a parapophysis
453 would have been located. The paired parapophyses normally ossify endochondrally from
454 basiventral cartilages ventrolateral to each centrum, whereas in *nkx3.2* mutants it appears
455 that this cartilage fails to form. This basiventral phenotype is reminiscent of the vertebral
456 defects identified in mouse mutants, namely that the ventromedial vertebral ossification

centres fail to form (Akazawa et al., 2000; Lettice et al., 1999; Tribioli and Lufkin, 1999). Similar defects in vertebral ossification have been identified in human patients suffering from SMMD, a disease caused by inactivating mutations in *NKX3.2* (Agarwal et al., 2003; Hellemans et al., 2009; Silverman and Reiley, 1985; Simon et al., 2012; Simsek-Kiper et al., 2019).

A major difference between the centra of teleosts and mammalian tetrapods is that the former directly ossify into bone without a cartilage precursor (Bensimon-Brito et al 2012), while the latter ossify endochondrally (Fleming et al, 2015). The cartilaginous vertebral precursors in tetrapods are derived from the sclerotome, while in zebrafish the notochord sheath mineralises to form chordacentra, followed by a sclerotome-derived intermembranous bone, forming autocentra (Bensimon-Brito et al., 2012; Fleming et al., 2004; Nordvik et al., 2005). Chondrichthyans and other non-tetrapod osteichthyans also form cartilaginous anlage of vertebral bodies, indicating that teleosts represent a derived condition (Criswell et al., 2017a; Peskin et al., 2020; Zhang, 2009). The basiventral and basidorsal cartilage elements in teleosts are derived also from the sclerotome (Criswell et al., 2017b; Gadow and Abbott, 1895). Our results are consistent with a role for Nkx3.2 in sclerotome-derived cartilage development in osteichthyans, rather than in vertebral development more generally. Thus, vertebrae-associated cartilages are affected in some way in the zebrafish, mouse, and human, but lead to different specific defects in teleosts compared to mammals as a result of these fundamental differences in vertebral development. Similar skeletal phenotypes are observed in knockouts of other transcription factors known to be involved in sclerotome patterning, such as Pax1 (Koseki et al., 1993; Wallin et al., 1994) and Gli2 (Mo et al., 1997).

Defects in the cervical vertebrae is another shared phenotype caused by *nkx3.2* mutations in the zebrafish, mouse, and human. In human SMMD patients, the reduced ossification of cervical vertebrae can lead to kinking of the neck (kyknodysostosis) and secondary neurological problems associated with an injured cervical cord (Simon et al., 2012). *Nkx3.2* knockout mouse embryos display a lack of chondrogenesis in the cervical vertebral bodies (Herbrand et al., 2002; Tribioli and Lufkin, 1999), and this is also likely the case in human SMMD embryos, part of the aetiology of the severe cervical defects seen postnatally. In zebrafish and other members of the teleost superorder Ostariophysi, especially otophysians, the cervical vertebrae and their associated elements have a unique structure collectively termed the Weberian apparatus (Grande and Young, 2004). This complex of bones is adapted for transmitting sound from the swim bladder to the inner ear along a chain of bony elements connected by ligaments. These bony elements represent highly derived cervical ribs and neural arches of vertebrae 1-4. In *nkx3.2* knockout zebrafish, we observed defects in all the ventral elements of the Weberian apparatus: lateral process 2, the tripus, and rib 4/os suspensorium. In the tripus and rib 4, the parts of these elements that are likely derived from basiventral cartilages - the anterior ramus of the tripus and both articulating processes - are absent or malformed such that the tripus and rib 4 are fused to cervical vertebrae 3 and 4 respectively, reminiscent of the phenotype in the other rib-bearing vertebrae as a result of the absence of parapophyses. Lateral process 2 on CV2 is absent or highly reduced in mutants. Dorsal elements of the Weberian apparatus, on the other hand, such as the supraneurals and neural arches, appear relatively unaffected. However, it is difficult to interpret the direct effects of *nkx3.2* knockout on the scaphium and claustrum because of the common loss of CV1 and the space dorsal to it that we suspect results from the

505 impaction of the cervical vertebrae into the occiput. These results further support an
506 essential role of Nkx3.2 that is restricted to the basiventral and not the basidorsal cartilage
507 in zebrafish.
508
509 Basiventral cartilage elements were once thought to be a gnathostome-specific feature until
510 it was revealed that hagfish, one of the two extant agnathan vertebrate taxa, possessed
511 basiventral elements (Ota et al., 2011). The lamprey, on the other hand, only possesses
512 basidorsal elements, leading to the hypothesis that this taxon secondarily lost basiventral
513 elements and that the ancestral vertebrate possessed both basiventral and basidorsal
514 elements (Ota et al., 2011). Studies on the involvement of Nkx3.2 in the development of
515 hagfish basiventral elements would shed light on its potentially pivotal role in this important
516 vertebrate innovation - was it essential in early vertebrates, or was it only recruited later in
517 the gnathostome lineage?
518
519 In the occiput of adult *nkx3.2* mutant zebrafish, we observed a partial or complete fusion
520 between the bones of the exoccipital and basioccipital that resulted in a partial or complete
521 loss of the cavum sinus impar. Our OPT results revealed a subtle but significant reduction in
522 cartilage staining intensity in this region at 5 dpf, which would have gone unnoticed
523 comparing individual images of the larvae by eye. These results highlight the utility of the
524 OPT method in identifying subtle phenotypes in larval stages, especially in cases where the
525 characterisation of adult phenotypes may not be possible. In mouse knockouts, these same
526 occipital bones are misshapen and underdeveloped (Akazawa et al., 2000; Lettice et al.,
527 1999; Tribioli and Lufkin, 1999), although fusions between them have not been described. In
528 addition, these *Nkx3.2* knockout mice display an absence of the supraoccipital bone, while

529 the supraoccipital in zebrafish appears to develop normally. There are no reports of any
530 defects to the occipital bones of human SMMD patients, although it is not clear whether this
531 is because no defects exist or because they have been overlooked, likely a result of the
532 difficulty in studying affected individuals *in utero* or shortly after birth.
533
534 In gnathostomes, the most anterior somites contribute to the occipital bones (Ferguson and
535 Graham, 2004; Maddin et al., 2020; Morin-Kensicki et al., 2002). The sclerotome from these
536 occipital somites contributes to the basioccipital and exoccipital (Couly et al., 1993; Müller
537 and O'Rahilly, 2003, 1994), so the occipital phenotypes observed in zebrafish and mouse
538 *nkx3.2/Nkx3.2* mutants are consistent with the role of Nkx3.2 in the sclerotome. The
539 combination of these occipital phenotypes, particularly the defects in the cavum sinus impar
540 and Weberian apparatus suggest that *nkx3.2* knockout zebrafish should have a severe
541 hearing impairment, which is supported by our anecdotal observations that larval mutants
542 fail to respond to tapping on their plates, while their heterozygous or wild-type siblings do.
543
544 *nkx3.2/Nkx3.2* expression has previously been identified in the median fins of zebrafish
545 (Crotwell and Mabee, 2007) and the limb buds and digits of mice (Akazawa et al., 2000;
546 Tribioli et al., 1997; Tribioli and Lufkin, 1999). We identified longer proximal radials, relative
547 to standard body length, in adult *nkx3.2* mutant zebrafish, which is consistent with results in
548 humans and mice. Like mammalian limb bones, teleost median proximal radials first develop
549 as hyaline cartilage before endochondral ossification takes place (Benjamin et al., 1992;
550 Konstantinidis and Conway, 2010). Human SMMD patients often display several limb defects
551 postnatally: long limbs, the presence of large epiphyses and irregular metaphyses that give
552 the disease its name, and the presence of pseudoepiphyses in the digits combined with

553 reduced ossification of the carpals (Agarwal et al., 2003; Hellemans et al., 2009; Silverman
554 and Reiley, 1985; Simon et al., 2012). Limb defects have not been reported in mouse
555 mutants (Herbrand et al., 2002; Lettice et al., 1999; Tribioli and Lufkin, 1999), but changes in
556 the regulation of *Nkx3.2* expression have been linked to tibia length (Castro et al., 2019),
557 suggesting that the gene has a similar role in humans and mice and that the reason limb
558 defects have not been found in mouse mutants is that the mutation is perinatally fatal, while
559 these limb phenotypes appear postnatally (Hellemans et al., 2009). These results are
560 consistent with a common role for Nkx3.2 in repressing chondrocyte maturation and
561 therefore endochondral bone formation, as downregulation or gene knockout results in
562 longer endochondral limb and median fin bones in all three species (Castro et al., 2019;
563 Hellemans et al., 2009), and *Nkx3.2* overexpression in mice causes the opposite - skeletal
564 dwarfism (Jeong et al., 2017).
565
566 The proximal radials of the dorsal and anal median fins develop with contributions from
567 somite-derived cells including the sclerotome (Freitas et al., 2006; Shimada et al., 2013),
568 while paired fins and limbs are derived from the lateral plate mesoderm (Shimada et al.,
569 2013; Zeller et al., 2009). Even though these different skeletal structures develop from
570 different progenitor populations, it has long been recognised that the paired limb buds
571 redeploy developmental mechanisms that first evolved in the median fins (Freitas et al.,
572 2006). Our results suggest that *nkx3.2* expression may have been co-opted from median fin
573 to limb development in the sarcopterygian lineage or even during the evolution of
574 tetrapods, as *nkx3.2* expression in actinopterygian paired fins has not been reported and we
575 were unable to identify any phenotypes in the paired fins of adult *nkx3.2* mutant
576 zebrafish. Definitive studies on the expression of *nkx3.2* in the fins of more basal

577 actinopterygians such as sturgeon, gar, and bichir, in addition to chondrichthyans, are
578 needed to provide a solid phylogenetic footing for this conclusion, as it may be that teleost
579 paired fins represent the derived state in this regard (Davis et al., 2007).
580
581 This study highlights the role of *nkx3.2* in the development of different skeletal tissues. In
582 the jaw and endochondral proximal radials, mutant phenotypes are consistent with a loss of
583 chondrocyte maturation inhibition, while in the basiventral cartilages along the precaudal
584 vertebrae, Nkx3.2 appears to be required for the onset or maintenance of cartilage
585 development. Comparing these results with studies of amniote model systems and human
586 disease reveal a largely consistent function of this gene between teleosts and amniotes,
587 suggesting their inheritance from an early osteichthyan ancestor. Future studies in
588 chondrichthyans and agnathans will further inform our understanding of the function of
589 Nkx3.2 in early vertebrate evolution.
590
591
592 **Materials and Methods**
593 *Ethical statement*
594 All animal experimental procedures were approved by the local ethics committee for animal
595 research in Uppsala, Sweden (permit number C161/4, 5.8.18-18096/2019). All procedures
596 for the experiments were performed in accordance with the animal welfare guidelines of the
597 Swedish National Board for Laboratory Animals.
598

599 *CRISPR/*Cas9 *target design*

600 Two sgRNAs targeting the single zebrafish *nkx3.2* gene with no predicted off-target effects
601 were designed using the online software CHOPCHOP (Labun et al., 2016), both targeting the
602 first exon: 5´-GATCAGGAATCCGCGGCCAA-3´ and 5´-GTCGTTGTCCTCGCTCAGCC-3´. The
603 second base of each target was modified to "G" in order to allow T7 transcription without
604 modifications. The sgRNAs were prepared as previously described (Varshney et al., 2015),
605 creating a fragment consisting of the T7 promotor, the targeted gene-specific sequence, and
606 the guide core sequence. The sgRNAs were synthesised by in vitro transcription using the
607 HiScribe T7 High Yield RNA Synthesis Kit (New England Biolabs, Ipswich, MA). Cas9 mRNA
608 was prepared by in vitro transcription with the mMESSAGE mMACHINE T3 Transcription Kit
609 (Life Technologies, Carlsbad, CA) using 500 ng of linearised plasmid that was retrieved from
610 5 µg of p-T3TS-nCas9n plasmid (plasmid #46757; Addgene, Cambridge, MA) digested with
611 XbaI (New England Biolabs, Ipswich, MA). The products were purified, and their integrity was
612 assessed using a denaturation gel.
613
614 *Generation of zebrafish mutant line*

615 Fertilised zebrafish (*Danio rerio*) eggs were obtained by natural spawning of *Tg(sox10:egfp)*
616 line (Carney et al., 2006). Embryos were injected at the one-cell stage with 150 pg of Cas9
617 mRNA and 50 pg of each sgRNA in RNase-free water as previously described (Varshney et al.,
618 2015), and maintained at 28.5°C in E3 medium (Westerfield, 2000). The efficiency of the
619 targets was estimated by the CRISPR-Somatic Tissue Activity Test (STAT) methodology in
620 eight embryos at two days post-injection, as previously described (Carrington et al., 2015).
621 The injected founder zebrafish (F0) were raised and incrossed. For genotyping the F1

zebrafish, DNA was extracted from a 1–3 mm amputation of the adult zebrafish caudal fin by lysing the tissue in 30 µl of 50 mM NaOH for 20 min at 95°C, adding 60 µl of 0.1 mM Tris and diluting the obtained material (1:10). For the initial genotyping step, FLA analysis was used. 2 µl of DNA (50–200 ng) was added to Platinum Taq DNA Polymerase. The PCR mix was incubated at 94°C for 12 min followed by 35 cycles of 94°C for 30 sec, 57°C for 30 sec, 72°C for 30 sec, and final extension at 72°C for 10 min. Size determination was carried out on a 3130XL ABI Genetic Analyzer (Applied Biosystems, Waltham, MA) and the data were analysed using the Peak Scanner Software (Thermo Fisher Scientific, Waltham, MA). For the fish that screened positive for the variant, the FLA results were confirmed by Sanger sequencing.

Founder screening and identification of heterozygous adult fish

One strain with an allele containing a frameshift deletion resulting in a premature stop codon (*nkx3.2*^{uu2803}) was selected for further experiments. The identified F1 founders were crossed with wild-type zebrafish (AB strain), and their adult offspring (F2) was genotyped. Heterozygous F2 fish of mutant line *nkx3.2*^{uu2803} were incrossed and the offspring was observed with bright-field and fluorescence microscopy. Embryos showing phenotypes were sacrificed and genotyped by FLA and/or Sanger sequencing (forward primer: 5'-TGTAAAAC-GACGGCCAGTGAGGAGTCTCGCCATCTGAA-3'; reverse primer: 5'-GTGTCTTACAGATGAA-GCTTTGAGTGGT-3').

643 *In vivo microscopy*

644 Fluorescent images were obtained with an inverted Leica TCS SP5 confocal microscope using
645 LAS-AF software (Leica Microsystems). Embryos were sedated with 0.16% MS-222 and
646 embedded in 0.8% low melting agarose onto the glass bottom of the 35mm dishes. To
647 prevent drying, embedded embryos were covered with system water containing 0.16% MS-
648 222. Screening for GFP in zebrafish larvae was performed using a Leica M205FCA
649 fluorescence microscope with the appropriate filter.

650

651 *Histological analysis*

652 Zebrafish juveniles and adults at 14, 30 and 90 dpf were fixed in 4% PFA and washed in PBST
653 buffer. 30 and 90 dpf fish were decalcified in 0.5 M EDTA for one week with EDTA exchange
654 every third day. Fish were transferred into 99.5% ethanol, followed by Xylene and
655 embedded into paraffin. Sagittal head sections of 6µm were prepared with Leica RM2155
656 Rotary Microtome. Tissue sections were deparaffinised with xylene and re-hydrated through
657 99.5% to 70% ethanol series and transferred to water. Sections were then stained with
658 Nuclear Fast Red (Vector Laboratories, Burlingame, CA) for 30 sec followed by a brief water
659 rinse and dehydration in 95% and 99.9% ethanol. Prior to mounting with VectaMount
660 (Vector Laboratories, Burlingame, CA), slides were washed in Clear-Rite 3 (Richard-Allan
661 Scientific, Kalamazoo, MI). Sections were imaged with 40x objective on Hamamatsu
662 NanoZoomer S60 Digital Slide Scanner.

663

664 *Skeletal staining*

665 Staining of cartilage and bone was done based on the previously published protocol by
666 Walker and Kimmel (2007). Zebrafish wild-type and mutant fish at 5, 9, 14 and 30 dpf were
667 euthanised, fixed in 4% PFA and transferred to 50% ethanol. For cartilage staining,
668 specimens were immersed in alcian blue solution (0.02% Alcian Blue 8 GX, 50mM MgCL2,
669 70% ethanol), and for bone staining, specimens were immersed in alizarin red solution (0.5%
670 Alizarin Red S). For double staining of cartilage and bone, specimens were immersed in
671 double staining solution (99% alcian blue solution, 1% alizarin red solution). After staining
672 overnight, specimens were washed twice with 50% ethanol and then immersed in water for
673 2 hours before being bleached in a solution of 1.5% H202 and 1% KOH until pigmentation
674 was removed. 30 dpf specimens were then immersed in trypsin solution (1% trypsin, 35%
675 sodium tetraborate) for 30 minutes followed by incubation in a solution of 10% glycerol and
676 0.5% KOH for 1 hour. All specimens were imaged with a Leica M205FCA microscope in a
677 solution of 50% glycerol and 0.25% KOH, followed by storage in 50% glycerol and 0.1% KOH.
678
679 *Optical Projection Tomography*
680 A custom-built Optical Projection Tomography (OPT) system was used for imaging of the
681 zebrafish embryos fixed at 5 dpf and stained with alcian blue (Sharpe et al., 2002; Zhang et
682 al., 2020). The OPT system, reconstruction algorithms, and alignment workflow were based
683 on the previously described method (Allalou et al., 2017). All embryos were kept in 99%
684 glycerol before they were loaded into the system for imaging. The rotational images were
685 acquired using a 3X telecentric objective with a pixel resolution of 1.15 µm/pixel. The
686 tomographic 3D reconstruction was done using a filtered back projection (FBP) algorithm in
687 MATLAB (Release R2015b; MathWorks, Natick, MA) together with the ASTRA Toolbox

(Palenstijn *et al*., 2013). For the data alignment, the registration toolbox elastix (Klein et al., 2010; Shamonin et al., 2014) was used. To reduce the computational time all 3D volumes in the registration were down-sampled to half the resolution.

The registration workflow was similar to the methods described by Allalou *et al.* (2017) where the wildtype fish were initially aligned and used to create an average reference fish using an Iterative Shape Averaging (ISA) algorithm (Rohlfing et al., 2001). All wild-type (*n*=10) and *nkx3.2*$^{uu2803/uu2803}$ (*n*=11) zebrafish were then aligned to the reference. After the alignment, a voxel-wise method was used to detect voxels that are significantly different between the groups. The Mann-Whitney U test was used to compare corresponding voxels in wild-type and mutant. The p-value threshold is set using a false discovery rate (FDR) (Noble, 2009) and a permutation test (Simpson et al., 2013). The FDR was set so that those random groupings showed only a small number of significant voxel differences ($p<2.5x10^{-4}$; FDR=0.045). All registration and analysis were done on the green channel of the RGB images.

Micro-computed tomography and segmentation

Five wild-type and five *nkx3.2*$^{uu2803/uu2803}$ zebrafish were fixed at 90 dpf and analysed with micro-computed tomography (µCT, SkyScan 1172, Bruker microCT, Belgium) at a voltage of 60 kV, a current of 167 µA, and an isotropic voxel size of 5.43 µm. Cross-sections were reconstructed using software package NRecon (NRecon 1.6.10, Bruker microCT, Belgium). The specimens were placed in 2mL Eppendorf tubes filled with 1% agarose and the 10ul pipette tip was used to keep the mouths of some wild-type fish in the open position. BMP image stacks obtained with µCT were imported into, segmented, and imaged using VGStudio MAX version 3.2.5 (Volume Graphics, Germany).

712

713 *Statistical analyses*

714 Proximal radial length measurements of 90dpf wild-type and *nkx3.2* mutant fish were
715 normalised by the standard length of the fish to give a scaled length in arbitrary units.
716 Graphs were prepared using the ggplot2 package (Wickham, 2016) in R (R Development Core
717 Team, 2020). A Wilcoxon test was used in the analysis.

718

719 Declaration of interest

720 The authors declare no conflicts of interest.

721

722 Author Contributions

723 TH, LW, and JL designed this project; all authors performed experimental work and analysed
724 the data; TH, LW, and JL wrote the paper with contributions from other authors.

725

726 Acknowledgements

727 TH was supported by Vetenskapsrådet (Starting grant 621-2012-4673). The development of
728 the OPT system was funded by a development project at SciLifeLab Uppsala (2017) and a
729 Technology Development grant at SciLifeLab (2018) both awarded to AA. VGStudio MAX
730 licence and some lab expenses were covered by a Wallenberg Scholarship awarded to Prof.
731 Per E. Ahlberg, who also offered thoughtful comments on the manuscript. We thank the
732 Genome Engineering Zebrafish facility in SciLifeLab Uppsala for generating CRISPR/Cas9
733 mutants, and Prof. Åsa Mackenzie for access to the Hamamatsu NanoZoomer S60 Digital
734 Slide Scanner.

References

Agarwal PP, Srinivasan A, Sharma R, Kabra M, Gupta AK. 2003. Spondylo-megaepiphyseal-metaphyseal dysplasia: An unusual bone dysplasia. *Pediatr Radiol* **33**:893–896. doi:10.1007/s00247-003-1033-3

Akazawa H, Komuro I, Sugitani Y, Yazaki Y, Nagai R, Noda T. 2000. Targeted disruption of the homeobox transcription factor Bapx1 results in lethal skeletal dysplasia with asplenia and gastroduodenal malformation. *Genes to Cells* **5**:499–513. doi:10.1046/j.1365-2443.2000.00339.x

Allalou A, Wu Y, Ghannad-Rezaie M, Eimon PM, Yanik MF. 2017. Automated deep-phenotyping of the vertebrate brain. *Elife* **6**:e23379. doi:10.7554/eLife.23379

Anthwal N, Joshi L, Tucker AS. 2013. Evolution of the mammalian middle ear and jaw: Adaptations and novel structures. *J Anat* **222**:147–160. doi:10.1111/j.1469-7580.2012.01526.x

Arnold CR, Lamont RE, Walker JT, Spice PJ, Chan CK, Ho CY, Childs SJ. 2015. Comparative analysis of genes regulated by Dzip1/iguana and hedgehog in Zebrafish. *Dev Dyn* **244**:211–223. doi:10.1002/dvdy.24237

Azpiazu N, Frasch M. 1993. Tinman and bagpipe: Two homeo box genes that determine cell fates in the dorsal mesoderm of Drosophila. *Genes Dev* **7**:1325–1340. doi:10.1101/gad.7.7b.1325

Benjamin M, Ralphs JR, Eberewariye OS. 1992. Cartilage and related tissues in the trunk and fins of teleosts. *J Anat* **181**:113–118.

Bensimon-Brito A, Cardeira J, Cancela M., Huysseune A, Witten P. 2012. Distinct patterns of notochord mineralization in zebrafish coincide with the localization of Osteocalcin isoform 1 during early vertebral centra formation. *BMC Dev Biol* **12**:28.

Carney TJ, Dutton KA, Greenhill E, Delfino-Machín M, Dufourcq P, Blader P, Kelsh RN. 2006. A direct role for Sox10 in specification of neural crest-derived sensory neurons. *Development* **133**:4619–4630. doi:10.1242/dev.02668

Caron MMJ, Emans PJ, Cremers A, Surtel DAM, Coolsen MME, van Rhijn LW, Welting TJM. 2013. Hypertrophic differentiation during chondrogenic differentiation of progenitor cells is stimulated by BMP-2 but suppressed by BMP-7. *Osteoarthr Cartil* **21**:604–613. doi:10.1016/j.joca.2013.01.009

Carrington B, Varshney GK, Burgess SM, Sood R. 2015. CRISPR-STAT: An easy and reliable PCR-based method to evaluate target-specific sgRNA activity. *Nucleic Acids Res* **43**:1–8. doi:10.1093/nar/gkv802

Castro JPL, Yancoskie MN, Marchini M, Belohlavy S, Hiramatsu L, Kučka M, Beluch WH, Naumann R, Skuplik I, Cobb J, Barton NH, Rolian C, Chan YF. 2019. An integrative genomic analysis of the longshanks selection experiment for longer limbs in mice. *Elife* **8**:e42014. doi:10.7554/eLife.42014.001

Cerny R, Cattell M, Sauka-Spengler T, Bronner-Fraser M, Yu F, Medeiros DM. 2010. Evidence for the prepattern/cooption model of vertebrate jaw evolution. *Proc Natl Acad Sci* **107**:17262–17267. doi:10.1073/pnas.1009304107

Couly GF, Coltey PM, Le Douarin NM. 1993. The triple origin of skull in higher vertebrates: A

777 study in quail-chick chimeras. *Development* **117**:409–429.

778 Criswell KE, Coates MI, Gillis JA. 2017a. Embryonic origin of the gnathostome vertebral
779 skeleton. *Proc R Soc B Biol Sci* **284**:1–7. doi:10.1098/rspb.2017.2121

780 Criswell KE, Coates MI, Gillis JA. 2017b. Embryonic development of the axial column in the
781 little skate, Leucoraja erinacea. *J Morphol* **278**:300–320. doi:10.1002/jmor.20637

782 Crotwell PL, Mabee PM. 2007. Gene expression patterns underlying proximal-distal skeletal
783 segmentation in late-stage zebrafish, Danio rerio. *Dev Dyn* **236**:3111–3128.
784 doi:10.1002/dvdy.21352

785 Davis MC, Dahn RD, Shubin NH. 2007. An autopodial-like pattern of Hox expression in the
786 fins of a basal actinopterygian fish. *Nature* **447**:473–476. doi:10.1038/nature05838

787 Ferguson CA, Graham A. 2004. Redefining the head-trunk interface for the neural crest. *Dev*
788 *Biol* **269**:70–80. doi:10.1016/j.ydbio.2004.01.013

789 Fleming A, Keynes R, Tannahill D. 2004. A central role for the notochord in vertebral
790 patterning. *Development* **131**:873–880. doi:10.1242/dev.00952

791 Freitas R, Zhang GJ, Cohn MJ. 2006. Evidence that mechanisms of fin development evolved
792 in the midline of early vertebrates. *Nature* **442**:1033–1037. doi:10.1038/nature04984

793 Gadow H, Abbott E. 1895. On the Evolution of the Vertebral Column of Fishes. *Philos Trans R*
794 *Soc Lond B Biol Sci* **186**:163–221.

795 Gidmark NJ, Staab KL, Brainerd EL, Hernandez LP. 2012. Flexibility in starting posture drives
796 flexibility in kinematic behavior of the kinethmoid-mediated premaxillary protrusion
797 mechanism in a cyprinid fish, Cyprinus carpio. *J Exp Biol* **215**:2262–2272.
798 doi:10.1242/jeb.070516

799 Grande T, Young B. 2004. The ontogeny and homology of the Weberian apparatus in the
800 zebrafish Danio rerio (Ostariophysi: Cypriniformes). *Zool J Linn Soc* **140**:241–254.
801 doi:10.1111/j.1096-3642.2003.00097.x

802 Hellemans J, Simon M, Dheedene A, Alanay Y, Mihci E, Rifai L, Sefiani A, van Bever Y, Meradji
803 M, Superti-Furga A, Mortier G. 2009. Homozygous Inactivating Mutations in the NKX3-2
804 Gene Result in Spondylo-Megaepiphyseal-Metaphyseal Dysplasia. *Am J Hum Genet*
805 **85**:916–922. doi:10.1016/j.ajhg.2009.11.005

806 Herbrand H, Pabst O, Hill R, Arnold HH. 2002. Transcription factors Nkx3.1 and Nkx3.2
807 (Bapx1) play an overlapping role in sclerotomal development of the mouse. *Mech Dev*
808 **117**:217–224. doi:10.1016/S0925-4773(02)00207-1

809 Jeong DU, Choi JY, Kim DW. 2017. Cartilage-Specific and Cre-Dependent Nkx3.2
810 Overexpression In Vivo Causes Skeletal Dwarfism by Delaying Cartilage Hypertrophy. *J*
811 *Cell Physiol* **232**:78–90. doi:10.1002/jcp.25446

812 Klein S, Staring M, Murphy K, Viergever MA, Pluim JPW. 2010. Elastix: A toolbox for intensity-
813 based medical image registration. *IEEE Trans Med Imaging* **29**:196–205.
814 doi:10.1109/TMI.2009.2035616

815 Konstantinidis P, Conway KW. 2010. The median-fin skeleton of the Eastern Atlantic and
816 Mediterranean clingfishes Lepadogaster lepadogaster (Bonnaterre) and Gouania
817 wildenowi (Risso) (Teleostei: Gobiesocidae). *J Morphol* **271**:215–224.

doi:10.1002/jmor.10792

Koseki H, Willin J, Wilting J, Mizutani Y, Kispert A, Ebensperger C, Herrmann BG, Christ B, Balling R. 1993. A role for Pax-1 as a mediator of notochordal signals during the dorsoventral specification of vertebrae. *Development* **119**:649–660.

Kuraku S, Takio Y, Sugahara F, Takechi M, Kuratani S. 2010. Evolution of oropharyngeal patterning mechanisms involving Dlx and endothelins in vertebrates. Dev Biol. **341(1)**:315-323. doi: 10.1016/j.ydbio.2010.02.013.

Labun K, Montague TG, Gagnon JA, Thyme SB, Valen E. 2016. CHOPCHOP v2: a web tool for the next generation of CRISPR genome engineering. *Nucleic Acids Res* **44**:W272–W276. doi:10.1093/nar/gkw398

Lengner CJ, Hassan MQ, Serra RW, Lepper C, Van Wijnen AJ, Stein JL, Lian JB, Stein GS. 2005. Nkx3.2-mediated repression of Runx2 promotes chondrogenic differentiation. *J Biol Chem* **280**:15872–15879. doi:10.1074/jbc.M411144200

Lettice LA, Purdie LA, Carlson GJ, Kilanowski F, Dorin J, Hill RE. 1999. The mouse bagpipe gene controls development of axial skeleton, skull, and spleen. *Proc Natl Acad Sci* **96**:9695–9700. doi:10.1073/pnas.96.17.9695

Lukas P, Olsson L. 2018a. Bapx1 is required for jaw joint development in amphibians. *Evol Dev* **20**:192–206. doi:10.1111/ede.12267

Lukas P, Olsson L. 2018b. Bapx1 upregulation is associated with ectopic mandibular cartilage development in amphibians. *Zool Lett* **4**:16. doi:10.1186/s40851-018-0101-3

Luo Z-X. 2011. Developmental Patterns in Mesozoic Evolution of Mammal Ears. *Annu Rev Ecol Evol Syst* **42**:355–380. doi:10.1146/annurev-ecolsys-032511-142302

Maddin HC, Piekarski N, Reisz RR, Hanken J. 2020. Development and evolution of the tetrapod skull–neck boundary. *Biol Rev* **95**:573–591. doi:10.1111/brv.12578

Miller CT, Yelon D, Stainier DYR, Kimmel CB. 2003. Two endothelin 1 effectors, hand2 and bapx1, pattern ventral pharyngeal cartilage and the jaw joint. *Development* **130**:1353–1365. doi:10.1242/dev.00339

Miyashita T, Baddam P, Smeeton J, Oel AP, Natarajan N, Gordon B, Palmer AR, Crump JG, Graf D, Allison WT. 2020. nkx3.2 mutant zebrafish accommodate the jaw joint loss through a phenocopy of the head shapes of Paleozoic jawless fish. *J Exp Biol* In Press. doi:10.1242/jeb.216945

Mo R, Freer AM, Zinyk DL, Crackower MA, Michaud J, Heng HHQ, Chik KW, Shi XM, Tsui LC, Cheng SH, Joyner AL, Hui CC. 1997. Specific and redundant functions of Gli2 and Gli3 zinc finger genes in skeletal patterning and development. *Development* **124**:113–123.

Morin-Kensicki EM, Melancon E, Eisen JS. 2002. Segmental relationship between somites and vertebral column in zebrafish. *Development* **129**:3851–3860.

Müller F, O'Rahilly R. 2003. Segmentation in staged human embryos: The occipitocervical region revisited. *J Anat* **203**:297–315. doi:10.1046/j.1469-7580.2003.00219.x

Müller F, O'Rahilly R. 1994. Occipitocervical segmentation in staged human embryos. *J Anat* **185**:251–258.

Nair S, Li W, Cornell R, Schilling TF. 2007. Requirements for Endothelin type-A receptors and

Endothelin-1 signaling in the facial ectoderm for the patterning of skeletogenic neural crest cells in zebrafish. *Development* **134**:335–345. doi:10.1242/dev.02704

Nichols JT, Pan L, Moens CB, Kimmel CB. 2013. Barx1 Represses Joints and Promotes Cartilage in the Craniofacial Skeleton. *Development* **140**:2765–75. doi:10.1242/dev.090639

Noble WS. 2009. How does multiple testing correction work? *Nat Biotechnol* **27**:1135–1137. doi:10.1038/nbt1209-1135

Nordvik K, Kryvi H, Totland GK, Grotmol S. 2005. The salmon vertebral body develops through mineralization of two preformed tissues that are encompassed by two layers of bone. *J Anat* **206**:103–114. doi:10.1111/j.1469-7580.2005.00372.x

Ota KG, Fujimoto S, Oisi Y, Kuratani S. 2011. Identification of vertebra-like elements and their possible differentiation from sclerotomes in the hagfish. *Nat Commun* **2**:373. doi:10.1038/ncomms1355

Palenstijn WJ, Batenburg KJ, Sijbers J. 2013. The ASTRA Tomography ToolboxProceedings of the 13th International Conference on Computational and Mathematical Methods in Science and Engineering.

Peskin B, Henke K, Cumplido N, Treaster S, Harris MP, Bagnat M, Arratia G. 2020. Notochordal Signals Establish Phylogenetic Identity of the Teleost Spine. *Curr Biol* **30**:2805–2814. doi:10.1016/j.cub.2020.05.037

Provot S, Kempf H, Murtaugh LC, Chung U, Kim DW, Chyung J, Kronenberg HM, Lassar AB. 2006. Nkx3.2/Bapx1 acts as a negative regulator of chondrocyte maturation. *Development* **133**:651–62. doi:10.1242/dev.02258

R Development Core Team R. 2020. R: A Language and Environment for Statistical Computing.

Rohlfing T, Brandt R, Maurer CR, Menzel R. 2001. Bee brains, B-splines and computational democracy: Generating an average shape atlasProceedings of the Workshop on Mathematical Methods in Biomedical Image Analysis. IEEE. pp. 187–194. doi:10.1109/mmbia.2001.991733

Schwend T, Ahlgren SC. 2009. Zebrafish con/disp1 reveals multiple spatiotemporal requirements for Hedgehog-signaling in craniofacial development. *BMC Dev Biol* **9**:59. doi:10.1186/1471-213X-9-59

Shamonin DP, Bron EE, Lelieveldt BPF, Smits M, Klein S, Staring M. 2014. Fast parallel image registration on CPU and GPU for diagnostic classification of Alzheimer's disease. *Front Neuroinform* **7**:50. doi:10.3389/fninf.2013.00050

Sharpe J, Ahlgren U, Perry P, Hill B, Ross A, Hecksher-Sørensen J, Baldock R, Davidson D. 2002. Optical projection tomography as a tool for 3D microscopy and gene expression studies. *Science (80-)* **296**:541–545. doi:10.1126/science.1068206

Shimada A, Kawanishi T, Kaneko T, Yoshihara H, Yano T, Inohaya K, Kinoshita M, Kamei Y, Tamura K, Takeda H. 2013. Trunk exoskeleton in teleosts is mesodermal in origin. *Nat Commun* **4**:1639. doi:10.1038/ncomms2643

Silverman FN, Reiley MA. 1985. Spondylo-Megaepiphyseal-Metaphyseal Dysplasia: A New Bone Dysplasia Resembling Cleidocranial Dysplasia. *Radiology* **156**:365–371.

doi:10.1111/j.1440-1673.1977.tb02961.x

Simon M, Campos-Xavier AB, Mittaz-Crettol L, Valadares ER, Carvalho D, Speck-Martins CE, Nampoothiri S, Alanay Y, Mihci E, van Bever Y, Garcia-Segarra N, Cavalcanti D, Mortier G, Bonafé L, Superti-Furga A. 2012. Severe neurologic manifestations from cervical spine instability in spondylo-megaepiphyseal-metaphyseal dysplasia. *Am J Med Genet Part C Semin Med Genet* **160 C**:230–237. doi:10.1002/ajmg.c.31339

Simpson SL, Lyday RG, Hayasaka S, Marsh AP, Laurienti PJ. 2013. A permutation testing framework to compare groups of brain networks. *Front Comput Neurosci* **7**:171. doi:10.3389/fncom.2013.00171

Simsek-Kiper PO, Kosukcu C, Akgun-Dogan O, Gocmen R, Utine GE, Soyer T, Korkmaz-Toygar A, Nishimura G, Alikasifoglu M, Boduroglu K. 2019. A novel NKX3-2 mutation associated with perinatal lethal phenotype of spondylo-megaepiphyseal-metaphyseal dysplasia in a neonate. *Eur J Med Genet* **62**:21–26. doi:10.1016/j.ejmg.2018.04.013

Square T, Jandzik D, Cattell M, Coe A, Doherty J, Medeiros DM. 2015. A gene expression map of the larval Xenopus laevis head reveals developmental changes underlying the evolution of new skeletal elements. *Dev Biol* **397**:293–304. doi:10.1016/j.ydbio.2014.10.016

Tribioli C, Frasch M, Lufkin T. 1997. Bapxl: an evolutionary conserved homologue of the Drosophila bagpipe homeobox gene is expressed in splanchnic mesoderm and the embryonic skeleton. *Mech Dev* **65**:145–162. doi:10.1016/S0925-4773(97)00067-1

Tribioli C, Lufkin T. 1999. The murine Bapx1 homeobox gene plays a critical role in embryonic development of the axial skeleton and spleen. *Development* **126**:5699–5711.

Tucker AS, Watson RP, Lettice LA, Yamada G, Hill RE. 2004. Bapx1 regulates patterning in the middle ear: altered regulatory role in the transition from the proximal jaw during vertebrate evolution. *Development* **131**:1235–1245. doi:10.1242/dev.01017

Varshney GK, Pei W, Lafave MC, Idol J, Xu L, Gallardo V, Carrington B, Bishop K, Jones M, Li M, Harper U, Huang SC, Prakash A, Chen W, Sood R, Ledin J, Burgess SM. 2015. High-throughput gene targeting and phenotyping in zebrafish using CRISPR/Cas9. *Genome Res* **25**:1030–1042. doi:10.1101/gr.186379.114

Walker MB, Kimmel CB. 2007. A two-color acid-free cartilage and bone stain for zebrafish larvae. *Biotech Histochem* **82**:23–28. doi:10.1080/10520290701333558

Wallin J, Wilting J, Koseki H, Fritsch R, Christ B, Balling R. 1994. The role of Pax-1 in axial skeleton development. *Development* **120**:1109–1121.

Weigele J, Franz-Odendaal TA. 2016. Functional bone histology of zebrafish reveals two types of endochondral ossification, different types of osteoblast clusters and a new bone type. *J Anat* **229**:92–103. doi:10.1111/joa.12480

Westerfield M. 2000. The Zebrafish Book: A Guide for the Laboratory Use of Zebrafish (Danio Rerio), 4th ed. Eugene: University of Oregon Press.

Westneat MW. 2006. Skull Biomechanics and Suction Feeding in Fishes In: Shadwick R, Lauder G, editors. Fish Biomechanics. pp. 29–75. doi:10.1016/S1546-5098(05)23002-9

Wickham H. 2016. ggplot2: Elegant Graphics for Data Analysis. Springer-Verlag New York.

942 Wilson J, Tucker AS. 2004. Fgf and Bmp signals repress the expression of Bapx1 in the
943 mandibular mesenchyme and control the position of the developing jaw joint. Dev Biol.
944 **266(1)**:138-150. doi: 10.1016/j.ydbio.2003.10.012.

945 Yamashita S, Andoh M, Ueno-Kudoh H, Sato T, Miyaki S, Asahara H. 2009. Sox9 directly
946 promotes Bapx1 gene expression to repress Runx2 in chondrocytes. *Exp Cell Res*
947 **315**:2231–2240. doi:10.1016/j.yexcr.2009.03.008

948 Zeller R, López-Ríos J, Zuniga A. 2009. Vertebrate limb bud development: Moving towards
949 integrative analysis of organogenesis. *Nat Rev Genet* **10**:845–858. doi:10.1038/nrg2681

950 Zhang G. 2009. An evo-devo view on the origin of the backbone: Evolutionary development
951 of the vertebrae. *Integr Comp Biol* **49**:178–186. doi:10.1093/icb/icp061

952 Zhang H, Waldmann L, Manuel R, Boije H, Haitina T, Allalou A. 2020. zOPT: an open source
953 optical projection tomography system and methods for rapid 3D zebrafish imaging.
954 Biomedical optics express **11(8)**: 4290-4305. doi: 10.1364/BOE.393519

955